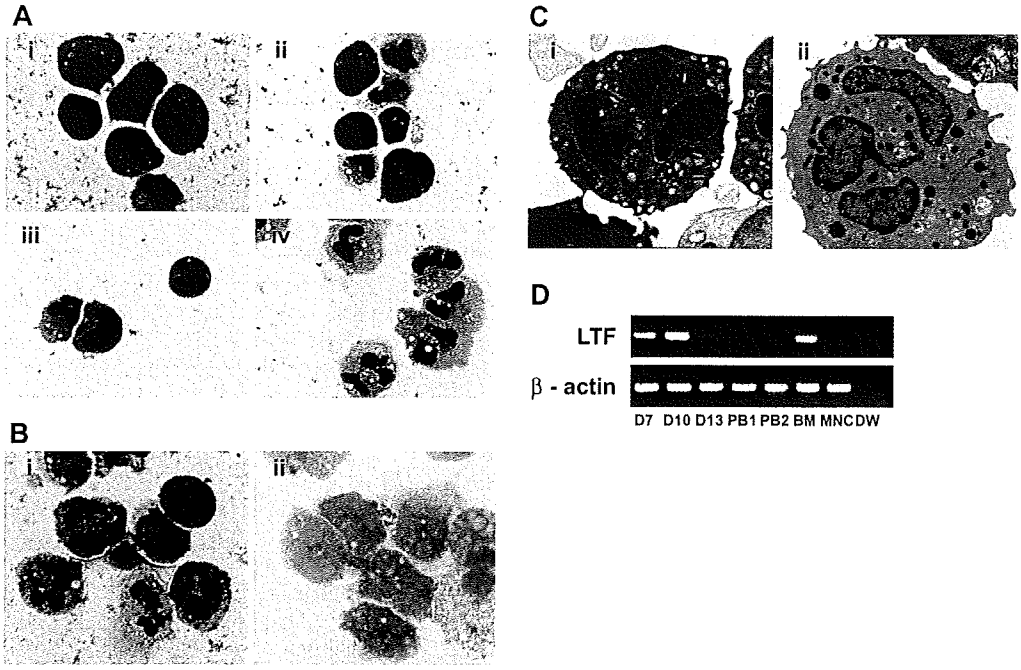

Figure 1. Morphology of hESC-derived cells and expression of lactoferrin mRNA. (A) Wright-Giemsa staining of the day-7 cells (i) revealed that they were morphologically myeloblasts and promyelocytes. On days 9 (ii) and 11 (iii), myelocytes and metamyelocytes were predominant, and on day 13 (iv; hESC-Neu), 70% to 80% of the cells appeared to be stab and segmented neutrophils. Original magnification, ×1000. (Bi) 97.3% plus or minus 1.5% of hESC-Neu's were myeloperoxidase positive. (ii) The neutrophil alkaline-phosphatase score in hESC-Neu's was 284 plus or minus 8.6. Values represent mean plus or minus SD. Original magnification, ×1000. (C) Microstructure of hESC-Neu's. Similar to steady-state neutrophils separated from peripheral blood (i), segmented nuclei and cytoplasmic granules were observed in hESC-Neu's (ii). Original magnification, ×8000. (D) Lactoferrin (LTF) mRNA was expressed in hESC-derived cells on day 7 (D7), peaked on day 10 (D10), and was weakly positive on day 13 (D13). Bone marrow mononuclear cells (BM) were strongly positive for LTF mRNA, but PB-Neu's (PB1 and 2) were negative, although faint bands were detected in PB-Neu's prepared from some donors (data not shown). As a negative control, peripheral blood mononuclear cells (MNCs) were used.

its expression was observed in less than 20% of the cells on day 7 and did not subsequently increase. CD16 (Fcγ receptor (FcγR) III), which is expressed in neutrophils as well as natural killer cells, macrophages, and a small subset of monocytes,[28] was already expressed by day 7, and increased with maturation. This expression pattern of CD16 is consistent with that during normal neutrophil differentiation, although the proportion of $CD16^-$ cells was lower than that of morphology-defined mature neutrophils on day 13. The ratio of CD32 (FcγRII)–positive cells increased as the differentiation stage advanced, and eventually reached 90%. CD64 (FcγRI) expression was greater than 80%, peaking on day 10, and the high percentage was maintained through day 13. CD14 was expressed in 20% to 25% of the cells on days 10 and 13.

Table 1. Differentiation pattern of hESC-derived cells

Cell type	% of total cells		
	Day 7	Day 10	Day 13
Myeloblasts	61.0 ± 9.1	2.3 ± 1.2	ND
Promyelocytes	16.8 ± 6.3	8.5 ± 0.9	0.7 ± 0.8
Myelocytes	12.3 ± 4.8	34.0 ± 6.8	6.4 ± 3.4
Metamyelocytes	3.0 ± 1.0	19.0 ± 1.3	10.2 ± 4.3
Stab neutrophils	0.8 ± 0.3	16.2 ± 3.0	18.3 ± 2.6
Segmented neutrophils	0.3 ± 0.6	14.7 ± 6.0	53.1 ± 9.6
Macrophage/monocytes	5.7 ± 0.6	5.3 ± 1.3	11.2 ± 1.4
Mature neutrophils	1.2 ± 0.8	30.8 ± 4.6	71.4 ± 7.4

The sum of the stab and segmented neutrophils indicates the total mature neutrophils. Data are shown as mean plus or minus SD (n = 3 independent experiments).

ND indicates not detectable.

In normal peripheral blood, both neutrophils and monocytes express CD15 and CD11b. In addition, mature neutrophils express CD16, whereas monocytes express CD14.[28,29] Detailed analysis on day 13 revealed that approximately 70% of $CD15^+$ and $CD11b^+$ cells were $CD16^+$, and almost all $CD15^+$ and $CD16^+$ cells expressed CD11b (Figure 2Bi,ii). Given that 70% to 80% of the cells on day 13 were morphologically mature neutrophils (Table 1), it is likely that the majority of hESC-Neu's had CD15, CD11b, and CD16 expression patterns similar to PB-Neu's, although some hESC-Neu's did not express CD15 or CD16, particularly CD16.

CD32 is broadly expressed on myeloid cells, whereas CD64 is expressed only on monocytes but not on neutrophils in the peripheral blood.[28] In the bone marrow, CD64 expression is observed in a small population of myeloblasts, peaks at the promyelocyte, myelocyte, and metamyelocyte stages, and then diminishes, although a small proportion of the stab neutrophils still express CD64.[30,31] We confirmed that virtually no PB-Neu's expressed CD64 (data not shown). In contrast, almost all $CD15^+$ and $CD16^+$ hESC-Neu's expressed CD64 on day 13, indicating that both stab and segmented hESC-Neu's expressed CD64, because segmented neutrophils represented more than 50% of the cells on day 13 (Figure 2Biii; Table 1). Nearly 50% of $CD15^+$ and $CD16^+$ cells were weakly positive for CD14, in contrast to the negative expression of CD14 in steady-state PB-Neu's (Figure 2Biv). This aberrant expression of CD64 and CD14 in hESC-Neu's is similar to their positive expression on some of the neutrophils harvested from healthy donors who received G-CSF administration[32,33] and the neutrophils derived from bone marrow $CD34^+$ cells in vitro by G-CSF stimulation.[31]

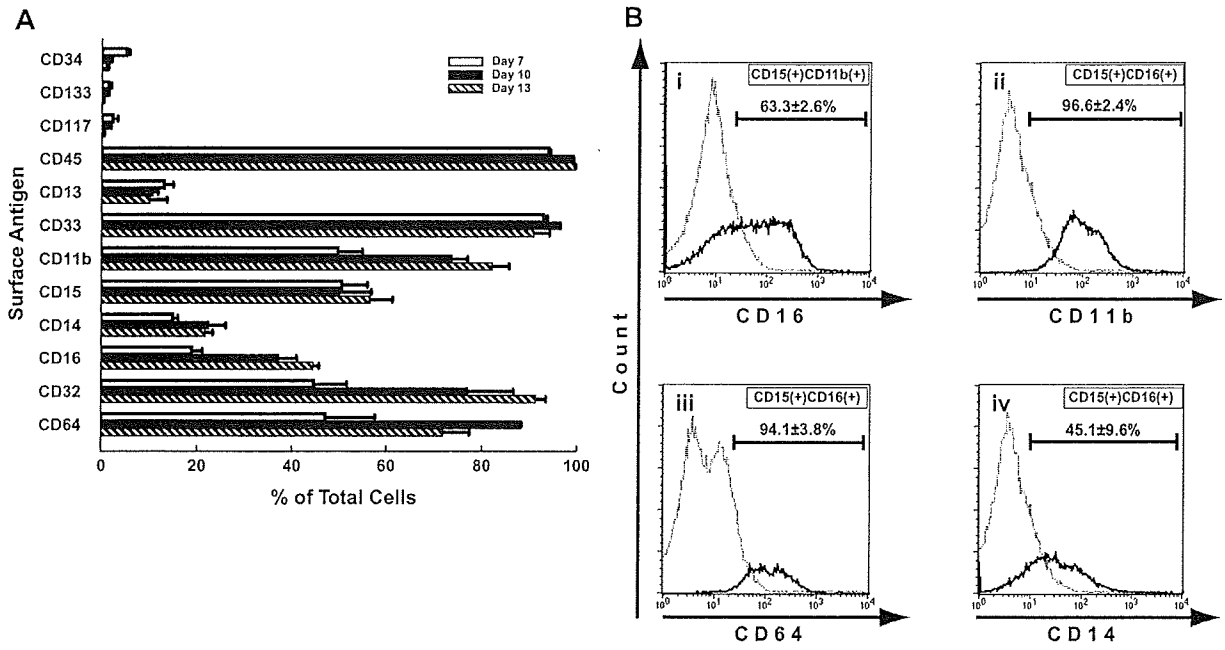

Figure 2. Surface antigens of hESC-derived cells. (A) Surface antigen expression at each level of differentiation of hESC-derived cells was analyzed by flow cytometry. CD45 was expressed in almost all the cells. CD34, CD117, and CD133, immature markers of hematopoiesis, were detected in a small population of the cells on day 7, and had almost disappeared by day 10. Common myeloid antigens CD33 and CD15 were highly expressed, and the expression of CD11b increased during maturation. CD13 was expressed in less than 20% of the cells throughout the culture period. The expression of CD16, a mature neutrophil marker, increased following maturation, but was observed in only approximately 45% of the cells, even on day 13. CD14 and CD64 expression was aberrantly observed in some cells. Bars represent SDs (n = 3). (B) In the steady state, mature neutrophils in peripheral blood were $CD15^+$, $CD11b^+$, and $CD16^+$. (i) In hESC-derived cells on day 13, 63.3% plus or minus 2.6% of the $CD15^+$ and $CD11b^+$ cells were $CD16^+$, and (ii) almost all of the $CD15^+$ and $CD16^-$ cells were $CD11b^+$. (iii-iv) On the other hand, CD64 and CD14 were rarely expressed on mature neutrophils in the peripheral blood. $CD15^+$ and $CD16^+$ cells from hESCs, consistent with the phenotype of mature neutrophils, showed aberrant expression of CD64 (iii) and CD14 (iv), in 94.1% plus or minus 3.8% and 45.1% plus or minus 9.6% of the cells, respectively. Data are presented as mean plus or minus SD (n = 3).

Apoptosis pattern and prolonged survival by G-CSF of hESC-Neu's and PB-Neu's

In the steady state, PB-Neu's have a short life span of approximately 24 hours, but this can be prolonged by G-CSF stimulation.[34] Some hESC-Neu's were already apoptotic at the time of harvest and therefore we focused on the nonapoptotic fraction of hESC-Neu's (Figure 3). In contrast to the PB-Neu's, which underwent apoptosis within 6 hours without G-CSF, consistent with previous reports,[34] a proportion of apoptotic cells among hESC-Neu's in the medium without G-CSF did not increase for up to 6 hours after the start of the culture. In addition, there were no differences between the cultures with and without G-CSF for up to 6 hours. After 6 hours, however, there was a more rapid decrease in nonapoptotic cells in hESC-Neu's without G-CSF than in hESC-Neu's with G-CSF, which resulted in a lower number of viable cells than hESC-Neu's with G-CSF at 24 hours, although the number of viable cells of hESC-Neu's without G-CSF was still higher than that of PB-Neu's without G-CSF.

Oxidative burst phenotype was similar in hESC-Neu's and PB-Neu's

Oxidative burst is an essential function of neutrophils when killing microorganisms, but an inappropriate burst sometime causes injury to the host tissue. We assessed the ability to convert DHR to rhodamine in hESC-Neu's and PB-Neu's using flow cytometry.[20] Because G-CSF, which could substantially affect the result, was used during the culture, we compared hESC-Neu's with PB-Neu(G+)'s and PB-Neu(G−)'s as described in "G-CSF stimulation prior to assessing neutrophil function." When DHR was added to the neutrophil suspensions, rhodamine-specific fluorescence was detected in hESC-Neu's, and in PB-Neu(G−)'s and PB-Neu(G+)'s without PMA stimulation, indicating basal superoxide production without PMA stimulation in each neutrophil preparation (Figure 4). PMA stimulation increased rhodamine mean fluorescence intensity in hESC-Neu's, but to a lesser extent than in PB-Neu(G−)'s and PB-Neu(G+)'s. Consequently, the mean rhodamine fluorescence intensity after PMA stimulation was similar in hESC-Neu's, PB-Neu(G−)'s, and PB-Neu(G+)'s, suggesting that the maximum superoxide production is comparable between hESC-Neu's and PB-Neu's.

Phagocytosis and subsequent NBT reduction activity, and bactericidal activity were similar between hESC-Neu's and PB-Neu's

Neutrophils protect against infectious microorganisms by phagocytosing and subsequently killing them. These functions of hESC-Neu's and PB-Neu's were evaluated in an experimental system using NBT-coated yeast. Under the microscope, mature neutrophils could be easily distinguished from contaminating macrophages by the unique shape of their nuclei after 1% safranin-O staining (Figure 5A). NBT-coated yeast that had not been ingested had a red-brown color that began to change to purple or black, beginning at the periphery, and eventually became completely black, because the NBT coating on the yeast was reduced by neutrophils after phagocytosis. Thus, neutrophils that had phagocytosis and NBT-reducing ability could be easily identified. hESC-Neu's had a slightly lower phagocytosis rate than PB-Neu(G−)'s and PB-Neu(G+)'s (Figure 5B). The phagocytosis score, however, was not significantly different between hESC-Neu's and PB-Neu(G−)'s and PB-Neu(G+)'s (Figure 5C). The cells on day 8 of the culture, most of which were morphologically myeloblasts and promyelocytes, were rarely observed

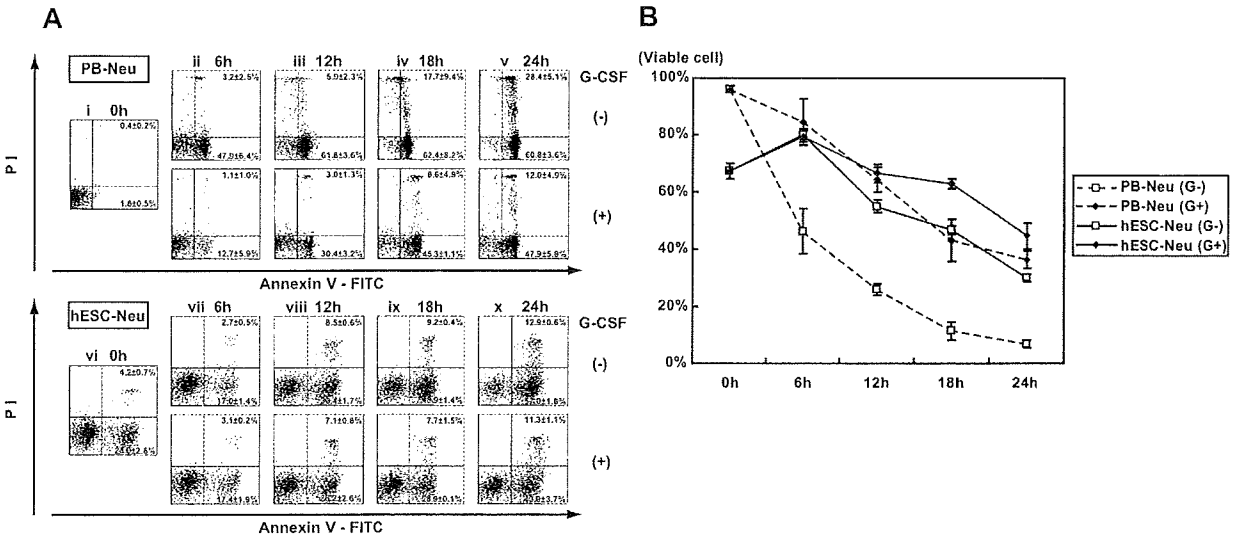

Figure 3. Apoptosis pattern and G-CSF effect on survival of hESC-Neu's. (A) Flow cytometric analysis. In the steady state, PB-Neu's have a short life span of approximately 24 hours, but this can be prolonged by G-CSF stimulation (i-v). Some hESC-Neu's were already apoptotic at the time of the harvest from the induction culture (vi). In contrast to the PB-Neu's that underwent apoptosis within 6 hours without G-CSF (ii), the proportion of apoptotic cells did not increase for up to 6 hours after the start of the culture of hESC-Neu's in the medium without G-CSF (vi,vii). In addition, there were no differences between the cultures of hESC-Neu's with and without G-CSF for up to 6 hours (vii). After 6 hours, nonapoptotic cells decreased more rapidly among hESC-Neu's without G-CSF than among hESC-Neu's with G-CSF (viii-x), resulting in the lower number of viable cells than hESC-Neu's with G-CSF at 24 hours (x). Figures are representative of 3 independent experiments. Data are presented as mean plus or minus SD (n = 3). (B) The time course of the decrease in viable cells. Bars represent SDs (n = 3).

to phagocytose the yeast or reduce NBT if they had ingested the yeast, indicating that we observed phagocytosis and NBT reduction that was specific to mature neutrophils.

Because the hESC-Neu's had sufficient phagocytosing ability and superoxide production, we next investigated whether hESC-Neu's can kill bacteria. The bactericidal activity of hESC-Neu's and PB-Neu's was compared using *E coli*. When incubated with hESC-Neu's and PB-Neu(G−)'s and PB-Neu(G+)'s, the numbers of CFUs were similarly reduced to approximately 40% that of the control, indicating comparable bactericidal activity against *E coli* between hESC-Neu's and PB-Neu's (Figure 5D).

Chemotaxis was similar between hESC-Neu's and PB-Neu's

We compared chemotaxis of hESC-Neu's and PB-Neu's using a modified Boyden chamber method. After incubation with or without fMLP in the lower well, neutrophils had migrated from the upper side to the lower side of the membrane. Neutrophil migration without fMLP in the lower well was considered random migration. The number of neutrophils that migrated randomly was not significantly different between hESC-Neu's and PB-Neu(G−)'s, but PB-Neu(G+)'s showed significantly more random migration than the others (Figure 5E). The number of migrated cells increased in hESC-Neu's, PB-Neu(G−)'s, and PB-Neu(G+)'s when fMLP was added in the lower well. The increase in cell migration induced by chemotaxis to fMLP was calculated by subtracting the number of randomly migrated cells without fMLP from that of migrated cells with fMLP. There were no significant differences between hESC-Neu's and PB-Neu(G−)'s or PB-Neu(G+)'s in the net fMLP-induced chemotaxis.

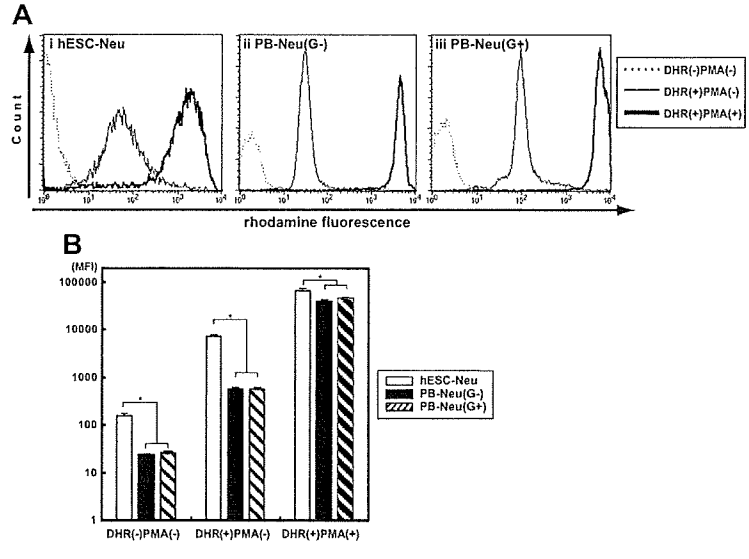

Figure 4. Superoxide production of hESC-Neu's assessed by dihydrorhodamine123 oxidation. (A) Dihydrorhodamine123 (DHR) was reacted to neutrophils with or without phorbol myristate acetate (PMA), and the resultant rhodamine fluorescence was detected by flow cytometry. When DHR was added to the reaction medium without PMA (line), the fluorescence levels were slightly elevated in hESC-Neu's (i), PB-Neu(G−)'s (ii), and PB-Neu(G+)'s (iii). The addition of PMA dramatically increased the levels of fluorescence in all 3 neutrophil preparations (bold line). The figures are representative of 3 independent experiments. (B) Comparison of superoxide production between hESC-Neu's and PB-Neu's using mean fluorescence intensity (MFI) of rhodamine. When DHR was added without PMA stimulation, rhodamine-specific fluorescence was detected in hESC-Neu's, PB-Neu(G−)'s, and PB-Neu(G−)'s. PMA stimulation increased rhodamine MFI in hESC-Neu's though to a lesser extent than in PB-Neu(G−)'s and PB-Neu(G+)'s. Consequently, rhodamine MFI after PMA stimulation was similar in hESC-Neu's, PB-Neu(G−)'s, and PB-Neu(G+)'s, suggesting that the maximum superoxide production was comparable between hESC-Neu's and PB-Neu's (n = 3; bars represent SDs; $^*P < .05$ compared with hESC-Neu's).

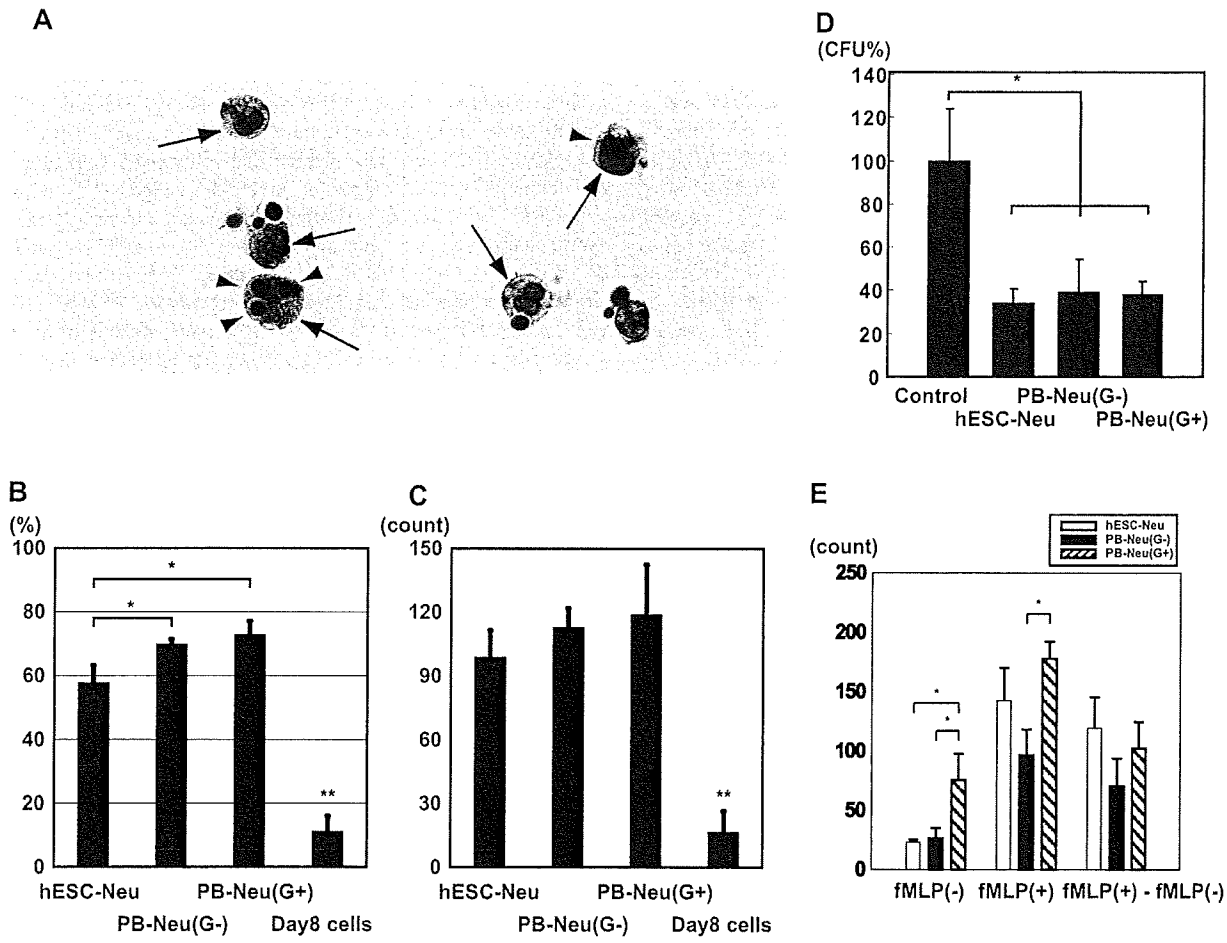

Figure 5. NBT-coated yeast cell-phagocytosis test, bactericidal activity, and chemotaxis assay. (A) NBT-coated yeast cells were added to a neutrophil suspension and incubated at 37°C. After 1 hour, the cells were stained with 1% safranin-O, and observed using a microscope. Mature neutrophils (→) could be easily distinguished from contaminating macrophages (white arrow; only the nucleus is observed in the figure) by the unique shape of their nuclei. Yeast cells were red-brown in color before being ingested (white arrowhead); the color began to change to purple or black beginning at the periphery of the yeast cell, and eventually became completely black (➤) because the NBT was reduced after ingestion. Yeast cells that changed color in the cells were counted as NBT-reduction positive. Original magnification, ×400. (B) The phagocytosis rate was calculated as a percentage of the neutrophils that contained one or more yeast cells. hESC-Neu's had a slightly lower phagocytosis rate than that of PB-Neu(G−)'s and PB-Neu(G+)'s. (C) The phagocytosis score was calculated as the total number of positive yeast cells in 100 neutrophils. There were no significant differences in the phagocytosis score between hESC-Neu's and PB-Neu(G−)'s or PB-Neu(G+)'s. The cells on day 8 of the culture (day-8 cells) were rarely observed to phagocytose the yeast cells or reduce NBT. (In B-C, n = 3; bars indicate SDs; $^*P < .05$ compared with PB-Neu(G−)'s and PB-Neu(G+)'s; $^{**}P < .05$ compared with hESC-Neu's, PB-Neu(G−)'s, and PB-Neu(G+)'s.) (D) Bactericidal assay. *E coli* was opsonized with human AB serum, and incubated with hESC-Neu's, PB-Neu(G−)'s, PB-Neu(G+)'s, or control medium. After 1-hour incubation with hESC-Neu's, PB-Neu(G−)'s, and PB-Neu(G+)'s, the colony-forming units (CFUs) were significantly reduced to approximately 40% of the control. There were no significant differences in bactericidal activity between hESC-Neu's, PB-Neu(G−)'s, and PB-Neu(G+)'s. The CFUs of controls are presented as 100% (n = 3; bars indicate SDs; $^*P < .05$ compared with control). (E) Chemotaxis assay by a modified Boyden chamber method. The number of neutrophils that migrated randomly (fMLP(−)) was not significantly different between hESC-Neu's and PB-Neu(G−)'s, but PB-Neu(G+)'s showed significantly greater random migration than hESC-Neu's and PB-Neu(G−)'s. The number of migrating cells increased in all hESC-Neu's, PB-Neu(G−)'s, and PB-Neu(G+)'s when fMLP was added to the lower well (fMLP(+)). The increase in the number of migrating cells induced by chemotaxis to fMLP (fMLP(+)-fMLP(−)) was not significantly different between hESC-Neu's and PB-Neu(G−)'s or PB-Neu(G+)'s (n = 3; bars indicate SDs; $^*P < .05$).

Discussion

We developed a specific and effective method for deriving mature neutrophils from hESCs, making it possible to analyze hESC-derived neutrophils in detail. hESC-derived neutrophils had characteristics similar to steady-state peripheral blood mature neutrophils in morphology and essential functions, although there were some differences in surface antigen expression.

Unfortunately, attempts to further purify the hESC-derived mature neutrophils from the hESC-Neu population by density gradient methods led to a massive reduction in cell yield. In the flow cytometric analysis, the mean intensity of hESC-Neu's in forward scatter was higher than that of PB-Neu's (data not shown), indicating that the size of morphologically mature neutrophils, comprising 70% to 80% of the hESC-Neu population, was larger than that of PB-Neu's. This finding indicates that the density of morphologically mature neutrophils in the hESC-Neu population was lower than that of PB-Neu's, which made it difficult to separate hESC-Neu's from other contaminating cells.

In this culture, we observed morphologically defined myeloblasts, promyelocytes, myelocytes, metamyelocytes, and, eventually, mature stab and segmented neutrophils, in this order, during the 13-day culture, which is similar to the granulocyte maturation process in bone marrow. The surface antigen expression pattern during differentiation was similar to that during normal granulopoiesis, with CD34 and CD117 expression on immature cells, and an increase in CD16 expression as differentiation advanced. Most

hESC-Neu's expressed CD16, CD15, CD11b, CD33, and CD45. This pattern is consistent with normal PB-Neu's, but the percentage of CD16-expressing cells was lower than that of mature neutrophils determined by morphology. The lower CD16 expression level is documented in neutrophils derived in vitro from bone marrow $CD34^+$ cells by stimulation with G-CSF, and is considered to be the effect of G-CSF on myeloid progenitors.[31] G-CSF also induces CD64 and CD14 expression on mature neutrophils,[31,35] and these effects are also observed in vivo when G-CSF is administered to healthy volunteers.[32,33] Therefore, the G-CSF present in the culture from day 7 may have affected the progenitors and led to the relatively low expression of CD16 on hESC-Neu's and aberrant expression of CD64 and CD14 on $CD15^+$ and $CD16^+$ hESC-Neu's.

In the apoptosis assay, some hESC-Neu's were already apoptotic at the time of the harvest from the induction culture, but the proportion of apoptotic cells among hESC-Neu's in the medium without G-CSF did not increase for up to 6 hours after the start of the culture. There are 2 possible reasons for the difference in the rate of apoptosis. First, the hESC-Neu's were more heterogeneous than the PB-Neu's, as they comprised cells at different stages from incompletely differentiated cells such as metamyelocytes to maturation-completed and aged neutrophils. Relatively immature cells or unaged mature neutrophils in the hESC-Neu population might have a longer lifespan than PB-Neu's. Second, the effect of G-CSF used in the induction culture might continue even after the washout.

In the chemotaxis assay, the random migration of hESC-Neu's was almost the same as that of PB-Neu(G−)'s, but lower than that of PB-Neu(G+)'s, although hESC-Neu's were stimulated by G-CSF before the assay. The effect of G-CSF on the random migration of neutrophils is controversial; random migration increases in vitro when neutrophils are stimulated by G-CSF,[36] whereas neutrophils obtained from G-CSF–treated patients with nonmyeloid malignancies show decreased random migration and chemotaxis.[37,38] Our in vitro experiment with PB-Neu(G+)'s and PB-Neu(G−)'s replicated the former result. Nevertheless, hESC-Neu's showed relatively low random migration despite stimulation with G-CSF, while maintaining almost normal fMLP-induced chemotaxis. One possible reason for these differences might be the continuous stimulation by G-CSF; hESC-Neu's were stimulated from the myeloblast stage, and thus, it was expected that the characteristics of the hESC-Neu's were more similar to those of neutrophils from G-CSF–stimulated donors rather than to normal mature neutrophils.

The low yield of hESC-Neu's is a major obstacle to their functional analysis in animals, and further, to their potential use in drug screening and clinical applications. The number of hESC-Neu's produced was less than twice that of the input EB-derived cells. Recently, erythroid progenitor cell lines that could differentiate into functional mature red blood cells both in vitro and in vivo were established from mouse ESCs.[39] In that report, the starting number of ESCs required to establish one progenitor line was 5×10^5, and transplantation of 2×10^7 cells of the progenitor line could ameliorate anemia in mice by increasing the red blood cell count. Similar methods could be considered in the granulopoiesis from hESCs. Another potential method is to use more immature or proliferation-competent cells than the cells with which we initiated the induction culture. One candidate may be hematopoietic progenitors that emerge in saclike structures derived from ESCs. In a report using cynomolgus monkey ESCs,[40] EBs were created and subsequently subjected to adherent culture on a gelatin-coated dish. After 2 weeks, saclike structures emerged that contained hematopoietic precursors at various stages of myeloid lineage. The authors mentioned the possible existence of hemangioblasts, because endothelial cells could be produced from those precursors under different conditions. Others have also reported similar saclike structures containing hematopoietic precursors created from hESCs.[10] In this paper, megakaryocytes were created from the inner cells, which were positive for hematoendothelial markers, such as CD34, CD31, vascular endothelial growth factor-receptor 2, and vascular endothelial-cadherin. These similar findings suggest that the cells in the saclike structures contain cells that are more immature than our EB-derived cells, and that the precursors inside the saclike structures have greater proliferation potency than our EB-derived cells. Because neither paper directly demonstrated the efficiency of mature blood cell production from monkey or human ES cells, however, the efficiency of producing neutrophils from our EB-derived cells should be compared with that from the saclike structure–derived cells.

Acknowledgments

We thank Dr Nakatsuji for providing the KhES-3, and Dr Nakano for providing the OP9 cells. We are grateful to Kyowa Hakko Kirin for providing TPO, FP6, and G-CSF, and to Kyokuto Pharmaceutical Industrial for the nonserum medium used in the EB formation. We also thank S. Ichimura for hESC culture.

This work was supported in part by a Grant-in-aid from the Japan Society of Promotion of Sciences (KAKENHI nos. 17390274, 18013012, 19390258, and 20015010); Research on Pharmaceutical and Medical Safety, Health and Labor Sciences Research Grants from the Ministry of Health, Labor and Welfare of Japan (H16-Iyaku-32); grants from the Astellas Foundation for Research on Metabolic Disorders; the Uehara Memorial Foundation; and the Sagawa Foundation for Promotion of Cancer Research (S.C.); and the Project for Realization of Regenerative Medicine (S.O.).

Authorship

Contribution: Y.Y. and T.S. performed the experiments; K.H. designed the NBT-coated yeast cell-phagocytosis test; M.S.-Y., and K.K. assisted with interpretation of experiments and provided insightful comments; Y.Y. interpreted the data, made the figures, and wrote the paper; T.T., M.K., and S.O. advised on experimental design; S.C. provided critical reading of the paper; T.S. and S.C. designed the research.

Conflict-of-interest disclosure: The authors declare no competing financial interests.

Correspondence: Shigeru Chiba, Department of Clinical and Experimental Hematology, University of Tsukuba, 1-1-1 Tennodai, Tsukuba, Ibaraki, 305-8575, Japan; e-mail: schiba-tky@umin.net.

References

1. Kaufman DS, Hanson ET, Lewis RL, Auerbach R, Thomson JA. Hematopoietic colony-forming cells derived from human embryonic stem cells. Proc Natl Acad Sci U S A. 2001;98:10716-10721.
2. Nakano T, Kodama H, Honjo T. Generation of lymphohematopoietic cells from embryonic stem cells in culture. Science. 1994;265:1098-1101.
3. Vodyanik MA, Bork JA, Thomson JA, Slukvin II. Human embryonic stem cell-derived CD34+ cells: efficient production in the coculture with OP9 stromal cells and analysis of lymphohematopoietic potential. Blood. 2005;105:617-626.

4. Chadwick K, Wang L, Li L, et al. Cytokines and BMP-4 promote hematopoietic differentiation of human embryonic stem cells. Blood. 2003;102: 906-915.
5. Cerdan C, Rouleau A, Bhatia M. VEGF-A165 augments erythropoietic development from human embryonic stem cells. Blood. 2004;103: 2504-2512.
6. Wang L, Menendez P, Shojaei F, et al. Generation of hematopoietic repopulating cells from human embryonic stem cells independent of ectopic HOXB4 expression. J Exp Med. 2005;201:1603-1614.
7. Keller G, Kennedy M, Papayannopoulou T, Wiles MV. Hematopoietic commitment during embryonic stem cell differentiation in culture. Mol Cell Biol. 1993;13:473-486.
8. Wang L, Li L, Shojaei F, et al. Endothelial and hematopoietic cell fate of human embryonic stem cells originates from primitive endothelium with hemangioblastic properties. Immunity. 2004;21: 31-41.
9. Lu SJ, Feng Q, Caballero S, et al. Generation of functional hemangioblasts from human embryonic stem cells. Nat Methods. 2007;4:501-509.
10. Takayama N, Nishikii H, Usui J, et al. Generation of functional platelets from human embryonic stem cells in vitro via ES-sacs, VEGF-promoted structures that concentrate hematopoietic progenitors. Blood. 2008;111:5298-5306.
11. Hübel K, Carter RA, Liles WC, et al. Granulocyte transfusion therapy for infections in candidates and recipients of HPC transplantation: a comparative analysis of feasibility and outcome for community donors versus related donors. Transfusion. 2002;42:1414-1421.
12. Mousset S, Hermann S, Klein SA, et al. Prophylactic and interventional granulocyte transfusions in patients with haematological malignancies and life-threatening infections during neutropenia. Ann Hematol. 2005;84:734-741.
13. Price TH. Granulocyte transfusion: current status. Semin Hematol. 2007;44:15-23.
14. Bhatia M. Hematopoietic development from human embryonic stem cells. Hematology Am Soc Hematol Educ Program. 2007;2007:11-16.
15. Suemori H, Yasuchika K, Hasegawa K, Fujioka T, Tsuneyoshi N, Nakatsuji N. Efficient establishment of human embryonic stem cell lines and long-term maintenance with stable karyotype by enzymatic bulk passage. Biochem Biophys Res Commun. 2006;345:926-932.
16. Thomson JA, Itskovitz-Eldor J, Shapiro SS, et al. Embryonic stem cell lines derived from human blastocysts. Science. 1998;282:1145-1147.
17. Suzuki T, Yokoyama Y, Kumano K, et al. Highly efficient ex vivo expansion of human hematopoietic stem cells using Delta1-Fc chimeric protein. Stem Cells. 2006;24:2456-2465.
18. Yuo A, Kitagawa S, Okabe T, et al. Recombinant human granulocyte colony-stimulating factor repairs the abnormalities of neutrophils in patients with myelodysplastic syndromes and chronic myelogenous leukemia. Blood. 1987;70:404-411.
19. Kumano K, Chiba S, Shimizu K, et al. Notch1 inhibits differentiation of hematopoietic cells by sustaining GATA-2 expression. Blood. 2001;98:3283-3289.
20. Vowells SJ, Sekhsaria S, Malech HL, Shalit M, Fleisher TA. Flow cytometric analysis of the granulocyte respiratory burst: a comparison study of fluorescent probes. J Immunol Methods. 1995; 178:89-97.
21. Richardson MP, Ayliffe MJ, Helbert M, Davies EG. A simple flow cytometry assay using dihydrorhodamine for the measurement of the neutrophil respiratory burst in whole blood: comparison with the quantitative nitrobluetetrazolium test. J Immunol Methods. 1998;219:187-193.
22. Emmendörffer A, Hecht M, Lohmann-Matthes ML, Roesler J. A fast and easy method to determine the production of reactive oxygen intermediates by human and murine phagocytes using dihydrorhodamine 123. J Immunol Methods. 1990; 131:269-275.
23. Decleva E, Menegazzi R, Busetto S, Patriarca P, Dri P. Common methodology is inadequate for studies on the microbicidal activity of neutrophils. J Leukoc Biol. 2006;79:87-94.
24. Harvath L, Falk W, Leonard EJ. Rapid quantitation of neutrophil chemotaxis: use of a polyvinylpyrrolidone-free polycarbonate membrane in a multiwell assembly. J Immunol Methods. 1980;37: 39-45.
25. Rado TA, Bollekens J, St Laurent G, Parker L, Benz EJ Jr. Lactoferrin biosynthesis during granulocytopoiesis. Blood. 1984;64:1103-1109.
26. Rado TA, Wei XP, Benz EJ Jr. Isolation of lactoferrin cDNA from a human myeloid library and expression of mRNA during normal and leukemic myelopoiesis. Blood. 1987;70:989-993.
27. Cowland JB, Borregaard N. The individual regulation of granule protein mRNA levels during neutrophil maturation explains the heterogeneity of neutrophil granules. J Leukoc Biol. 1999;66:989-995.
28. van de Winkel JG, Anderson CL. Biology of human immunoglobulin G Fc receptors. J Leukoc Biol. 1991;49:511-524.
29. van Lochem EG, van der Velden VH, Wind HK, te Marvelde JG, Westerdaal NA, van Dongen JJ. Immunophenotypic differentiation patterns of normal hematopoiesis in human bone marrow: reference patterns for age-related changes and disease-induced shifts. Cytometry B Clin Cytom. 2004;60:1-13.
30. Ball ED, McDermott J, Griffin JD, Davey FR, Davis R, Bloomfield CD. Expression of the three myeloid cell-associated immunoglobulin G Fc receptors defined by murine monoclonal antibodies on normal bone marrow and acute leukemia cells. Blood. 1989;73:1951-1956.
31. Kerst JM, van de Winkel JG, Evans AH, et al. Granulocyte colony-stimulating factor induces hFc gamma RI (CD64 antigen)-positive neutrophils via an effect on myeloid precursor cells. Blood. 1993;81:1457-1464.
32. Kerst JM, de Haas M, van der Schoot CE, et al. Recombinant granulocyte colony-stimulating factor administration to healthy volunteers: induction of immunophenotypically and functionally altered neutrophils via an effect on myeloid progenitor cells. Blood. 1993;82:3265-3272.
33. Carulli G. Effects of recombinant human granulocyte colony-stimulating factor administration on neutrophil phenotype and functions. Haematologica. 1997;82:606-616.
34. van Raam BJ, Drewniak A, Groenewold V, van den Berg TK, Kuijpers TW. Granulocyte colony-stimulating factor delays neutrophil apoptosis by inhibition of calpains upstream of caspase-3. Blood. 2008;112:2046-2054.
35. Kerst JM, Slaper-Cortenbach IC, von dem Borne AE, van der Schoot CE, van Oers RH. Combined measurement of growth and differentiation in suspension cultures of purified human CD34-positive cells enables a detailed analysis of myelopoiesis. Exp Hematol. 1992;20:1188-1193.
36. Nakamae-Akahori M, Kato T, Masuda S, et al. Enhanced neutrophil motility by granulocyte colony-stimulating factor: the role of extracellular signal-regulated kinase and phosphatidylinositol 3-kinase. Immunology. 2006;119:393-403.
37. Azzarà A, Carulli G, Rizzuti-Gullaci A, Minnucci S, Capochiani E, Ambrogi F. Motility of rhG-CSF-induced neutrophils in patients undergoing chemotherapy: evidence for inhibition detected by image analysis. Br J Haematol. 1996;92:161-168.
38. Ribeiro D, Veldwijk MR, Benner A, et al. Differences in functional activity and antigen expression of granulocytes primed in vivo with filgrastim, lenograstim, or pegfilgrastim. Transfusion. 2007: 47:969-980.
39. Hiroyama T, Miharada K, Sudo K, Danjo I, Aoki N, Nakamura Y. Establishment of mouse embryonic stem cell-derived erythroid progenitor cell lines able to produce functional red blood cells. PLoS ONE. 2008;3:e1544.
40. Nakahara M, Matsuyama S, Saeki K, et al. A feeder-free hematopoietic differentiation system with generation of functional neutrophils from feeder- and cytokine-free primate embryonic stem cells. Cloning Stem Cells. 2008;10:341-354.

nature

Vol 460|13 August 2009|doi:10.1038/nature08240

LETTERS

Gain-of-function of mutated *C-CBL* tumour suppressor in myeloid neoplasms

Masashi Sanada[1,5]*, Takahiro Suzuki[7]*, Lee-Yung Shih[8]*, Makoto Otsu[9], Motohiro Kato[1,2], Satoshi Yamazaki[6], Azusa Tamura[1], Hiroaki Honda[11], Mamiko Sakata-Yanagimoto[12], Keiki Kumano[3], Hideaki Oda[13], Tetsuya Yamagata[14], Junko Takita[1,2,3], Noriko Gotoh[10], Kumi Nakazaki[1,4], Norihiko Kawamata[15], Masafumi Onodera[16], Masaharu Nobuyoshi[7], Yasuhide Hayashi[17], Hiroshi Harada[18], Mineo Kurokawa[3,4], Shigeru Chiba[12], Hiraku Mori[18], Keiya Ozawa[7], Mitsuhiro Omine[18], Hisamaru Hirai[3,4], Hiromitsu Nakauchi[6,9], H. Phillip Koeffler[15] & Seishi Ogawa[1,5]

Acquired uniparental disomy (aUPD) is a common feature of cancer genomes, leading to loss of heterozygosity. aUPD is associated not only with loss-of-function mutations of tumour suppressor genes[1], but also with gain-of-function mutations of proto-oncogenes[2]. Here we show unique gain-of-function mutations of the *C-CBL* (also known as *CBL*) tumour suppressor that are tightly associated with aUPD of the 11q arm in myeloid neoplasms showing myeloproliferative features. The *C-CBL* proto-oncogene, a cellular homologue of *v-Cbl*, encodes an E3 ubiquitin ligase and negatively regulates signal transduction of tyrosine kinases[3–6]. Homozygous *C-CBL* mutations were found in most 11q-aUPD-positive myeloid malignancies. Although the *C-CBL* mutations were oncogenic in NIH3T3 cells, c-Cbl was shown to functionally and genetically act as a tumour suppressor. C-CBL mutants did not have E3 ubiquitin ligase activity, but inhibited that of wild-type C-CBL and CBL-B (also known as CBLB), leading to prolonged activation of tyrosine kinases after cytokine stimulation. *c-Cbl*$^{-/-}$ haematopoietic stem/progenitor cells (HSPCs) showed enhanced sensitivity to a variety of cytokines compared to *c-Cbl*$^{+/+}$ HSPCs, and transduction of *C-CBL* mutants into *c-Cbl*$^{-/-}$ HSPCs further augmented their sensitivities to a broader spectrum of cytokines, including stem-cell factor (SCF, also known as KITLG), thrombopoietin (TPO, also known as THPO), IL3 and FLT3 ligand (FLT3LG), indicating the presence of a gain-of-function that could not be attributed to a simple loss-of-function. The gain-of-function effects of C-CBL mutants on cytokine sensitivity of HSPCs largely disappeared in a *c-Cbl*$^{+/+}$ background or by co-transduction of wild-type *C-CBL*, which suggests the pathogenic importance of loss of wild-type *C-CBL* alleles found in most cases of *C-CBL*-mutated myeloid neoplasms. Our findings provide a new insight into a role of gain-of-function mutations of a tumour suppressor associated with aUPD in the pathogenesis of some myeloid cancer subsets.

Myelodysplastic syndromes (MDS) are heterogeneous groups of blood cancers originating from haematopoietic precursors. They are characterized by deregulated haematopoiesis showing a high propensity to acute myeloid leukaemia (AML)[7]. Some MDS cases have overlapping clinico-pathological features with myeloproliferative disorders, and are now classified into myelodysplasia/myeloproliferative neoplasms (MDS/MPN) by the World Health Organization (WHO) classification[8]. To obtain a comprehensive profile of allelic imbalances in these myeloid neoplasms, we performed allele-specific copy number analyses of bone marrow samples obtained from 222 patients with MDS, MDS/MPN, or other related myeloid neoplasms (Supplementary Tables 1 and 2) using high-density single nucleotide polymorphism (SNP) arrays combined with CNAG/AsCNAR software[9,10].

Genomic profiles of MDS and MDS/MPN showed characteristic unbalanced genetic changes, as reported in previous cytogenetic studies[11] (Supplementary Fig. 1a); however, they were detected more sensitively by SNP array analyses (Supplementary Table 3). aUPD was detected in 70 samples (31.5%) on the basis of the allele-specific copy number analyses, which substantially exceeded the detection rate obtained using a SNP call-based detection algorithm (20.7%) (Supplementary Figs 2 and 4, and Supplementary Tables 4 and 5). Long stretches of homozygous SNP calls caused by shared identical-by-descent alleles in parents were empirically predicted and excluded (Supplementary Fig. 3). aUPDs were more common in MDS/MPN than in MDS. They preferentially affected several chromosomal arms (1p, 1q, 4q, 7q, 11p, 11q, 14q, 17p and 21q) in distinct subsets of patients, and frequently associated with mutated oncogenes and tumour suppressor genes (Supplementary Figs 1b and 5). Among these, the most common aUPDs were those involving 11q ($n = 17$), which defined a unique subset of myeloid neoplasms that were clinically characterized by frequent diagnosis of chronic myelomonocytic leukaemia (CMML) with normal karyotypes (13 cases) (Fig. 1a and Supplementary Table 6). We identified a minimum overlapping aUPD segment of approximately 1.4 megabases (Mb) in 11q, which contained a mutated *C-CBL* proto-oncogene (Fig. 1b).

[1]Cancer Genomics Project, [2]Department of Pediatrics, [3]Cell Therapy and Transplantation Medicine, and [4]Hematology and Oncology, Graduate School of Medicine, The University of Tokyo, 7-3-1 Hongo, Bunkyo-ku, Tokyo 113-8655, Japan. [5]Core Research for Evolutional Science and Technology, [6]Exploratory Research for Advanced Technology, Japan Science and Technology Agency, 4-1-8 Honcho, Kawaguchi-shi, Saitama 332-0012, Japan. [7]Division of Hematology, Department of Medicine, Jichi Medical University, 3311-1 Yakushiji, Shimotsuke-shi, Tochigi 329-0498, Japan. [8]Division of Hematology-Oncology, Department of Internal Medicine, Chang Gung Memorial Hospital, Chang Gung University, 199 Tung Hwa North Road, Taipei 105, Taiwan. [9]Division of Stem Cell Therapy, Center for Stem Cell and Regenerative Medicine, [10]Division of Systems Biomedical Technology, Institute of Medical Science, The University of Tokyo, 4-6-1 Shirokanedai, Minato-ku, Tokyo 108-8639, Japan. [11]Department of Developmental Biology, Research Institute of Radiation Biology and Medicine, Hiroshima University, 1-2-3 Kasumi, Minami-ku, Hiroshima 734-8553, Japan. [12]Department of Clinical and Experimental Hematology, Institute of Clinical Medicine, University of Tsukuba, 1-1-1 Tennodai, Tukuba-shi, Ibaraki, 305-8571, Japan. [13]Department of Pathology, Tokyo Women's Medical University, 8-1 Kawada-cho, Shinjuku-ku, Tokyo 162-8666, Japan. [14]Department of Hematology, Dokkyo University School of Medicine, 800 Kitabayashi, Mibu, Tochigi 321-0293, Japan. [15]Hematology/Oncology, Cedars-Sinai Medical Center, 8700 Beverly Boulevard, Los Angeles, California 90048, USA. [16]Department of Genetics, National Research Institute for Child Health and Development, 2-10-1 Okura, Setagaya-ku, Tokyo, 157-8535, Japan. [17]Gunma Children's Medical Center, 779 Shimohakoda, Hokkitsu-machi, Shibukawa-shi, Gunma 377-8577, Japan. [18]Division of Hematology, Internal Medicine, Showa University Fujigaoka Hospital, 1-30 Fujigaoka, Aoba-ku, Yokohama, Kanagawa 227-8501, Japan.
*These authors contributed equally to this work.

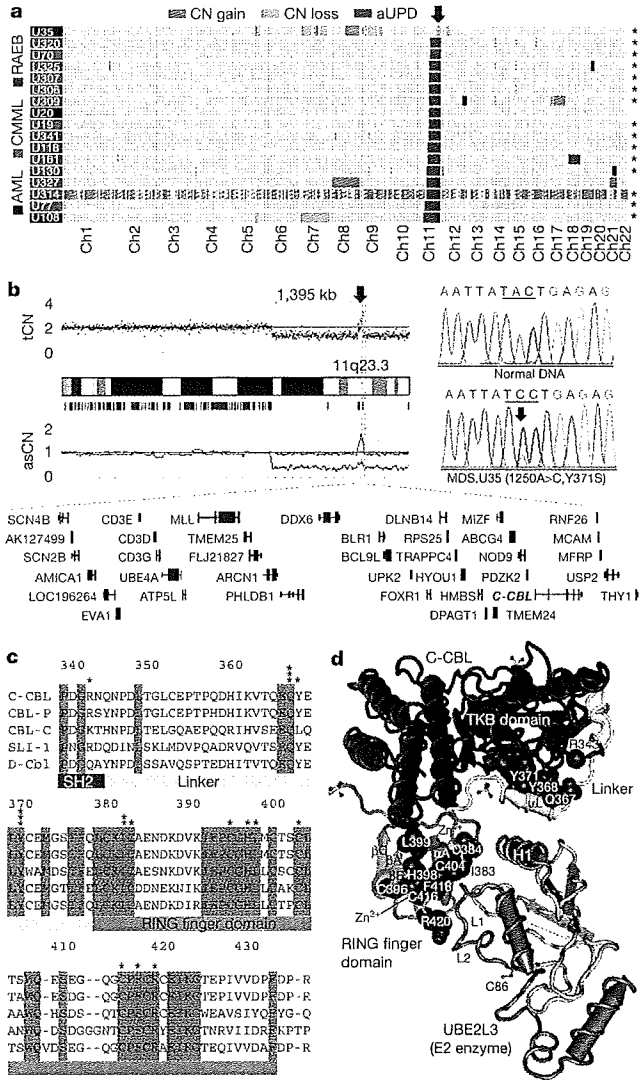

Figure 1 | Common UPD on the 11q arm and *C-CBL* mutations in myeloid neoplasms. **a**, Copy number profiles of 17 cases with myeloid neoplasms showing 11qUPD. Regions of copy number (CN) gains, losses and aUPD are depicted in different colours. Histologies are shown by coloured boxes. Asterisks denote *C-CBL*-mutated cases. Ch, chromosome; RAEB, refractory anaemia with excess blasts. **b**, CNAG output for MDS.U35. Total copy number (tCN) and allele-specific copy number (asCN) plots show a focal copy number gain spanning a 1.4-Mb segment within 3 Mb of an 11q-aUPD region (left), which contained mutated *C-CBL* in MDS.U35 (right). **c**, Alignments of amino acid sequences for human CBL family proteins and their homologues in *Caenorhabditis elegans* (SLI-1) and *Drosophila* (D-Cbl). Amino acid numbering is on the basis of human *C-CBL*. Conserved amino acids are highlighted. Positions of mutated amino acids are indicated by asterisks. Heterozygous mutations are shown in red. **d**, Mutated amino acid positions in the three-dimensional structure of a human C-CBL–UBE2L3 complex. TKB, tyrosine kinase binding domain.

C-CBL is the cellular homologue of the *v-Cbl* transforming gene of the Cas NS-1 murine leukaemia virus[5,12]. It was recently found to be mutated in human AML cases[13–15]. Together with its close homologue, CBL-B, C-CBL is thought to be involved in the negative modulation of tyrosine kinase signalling, primarily through their E3 ubiquitin ligase activity that is responsible for the downregulation of activated tyrosine kinases[3–5]. By sequencing all *C-CBL* exons in all 222 samples, we found *C-CBL* mutations in 15 of the 17 cases with 11q-aUPD, whereas only 3 out of 205 cases without 11q-aUPD had *C-CBL* mutations, showing a strong association of *C-CBL* mutations with 11q-aUPD ($P = 1.46 \times 10^{-18}$) (Supplementary Fig. 6 and Supplementary Tables 6 and 7), as also indicated in a recent report[16]. Thus, *C-CBL* was thought to be the major, if not the only, target of 11q-aUPD in myeloid neoplasms. Two different *C-CBL* mutations co-existed in three cases (Supplementary Fig. 6b). Somatic origins of the mutations were confirmed in three evaluable cases (Supplementary Fig. 6c).

In most cases, *C-CBL* mutations were missense, involving the evolutionarily conserved amino acids within the linker-RING finger domain that is central to the E3 ubiquitin ligase activity[17] (Fig. 1c). Another case with a predominant Cys384Tyr mutation also contained a nonsense mutation (Arg343X) in a minor subclone, which resulted in a v-Cbl-like truncated protein (Supplementary Fig. 6b). In the remaining two cases, mutations led to amino acid deletions (Δ369−371 and Δ368−382) involving the highly conserved α-helix (αL) of the linker domain and the first loop of the RING finger. According to the published crystal structure of *C-CBL*[17], most of the mutated or deleted amino acids were positioned on the interface for the binding to the E2 enzyme (Fig. 1d), making contact with either the tyrosine kinase binding domain (Tyr 368 and Tyr 371) or E2 ubiquitin-conjugating enzymes (Ile 383, Cys 404 and Phe 418). Especially, all seven linker-domain mutations selectively involved just three amino acids (Gln 367, Tyr 368 and Tyr 371) within the conserved αL helix (Fig. 1d). Mutations were clearly homozygous in nine cases, and the apparently heterozygous chromatograms in the other six cases could also be compatible with homozygous mutations affecting the aUPD-positive tumour clones, given the presence of substantial normal cell components within these samples. Mutations in the remaining three cases were considered to be heterozygous. About half of the *C-CBL*-mutated cases carried coexisting mutations of *RUNX1* (four cases), *TP53* (one case), *FLT3* internal tandem duplication (1 case) or *JAK2* (3 cases). *NRAS* and *KRAS* mutations were prevalent among CMML (15.1%) but occurred within discrete clusters from *C-CBL*-mutated cases (Supplementary Tables 2 and 6 and Supplementary Fig. 5). The mutation status of *C-CBL* did not substantially affect the clinical outcome (Supplementary Fig. 7).

All tested *C-CBL* mutants induced clear oncogenic phenotypes in NIH3T3 fibroblasts, as demonstrated by enhanced colony formation in soft agar and tumour generation in nude mice (Supplementary Fig. 8). Transformed NIH3T3 cells showed PI3 kinase-dependent activation of Akt and the transformed phenotype was reverted by treatment with the PI3 kinase inhibitor Ly294002 (Supplementary Fig. 9). When introduced into $Lin^-Sca1^+c\text{-}Kit^+$ (LSK) HSPCs, C-CBL mutants (C-CBL(Gln367Pro) and C-CBL(Tyr371Ser)), as well as a mouse lymphoma-derived oncogenic mutant (C-CBL(70Z)), significantly promoted the replating capacity of these progenitors (Fig. 2a). Because c-Cbl negatively modulates tyrosine kinase signalling, and all *C-CBL* mutations, including those previously reported[13–16], affected the critical domains for its enzymatic activity involved in this modulation, C-CBL was postulated to have a tumour suppressor function; loss-of-function could be a mechanism for the oncogenicity of these C-CBL mutants[3,5]. To assess this possibility and to clarify further the role of *C-CBL* mutations in the pathogenesis of myeloid neoplasms, we generated *c-Cbl*$^{-/-}$ mice and examined their haematological phenotypes (Supplementary Fig. 10).

In agreement with previous reports[18–20], *c-Cbl*$^{-/-}$ mice exhibited splenomegaly and an augmented haematopoietic progenitor pool, as was evident from the increased colony formation of bone marrow cells in methylcellulose culture and higher numbers of LSK and CD34-negative LSK cells in bone marrow and/or spleen compared to their wild-type littermates (Fig. 2b–d and Supplementary Fig. 11). Furthermore, when introduced into a *BCR-ABL* transgenic background[21], the *c-Cbl*$^{-/-}$ allele accelerated blastic crisis depending on the allele dosage (Fig. 2e, f). These observations supported the notion that wild-type *C-CBL* has tumour suppressor functions, whereas 'mutant' *C-CBL* acts as an oncogene; *C-CBL* can therefore be both a proto-oncogene and a tumour suppressor gene.

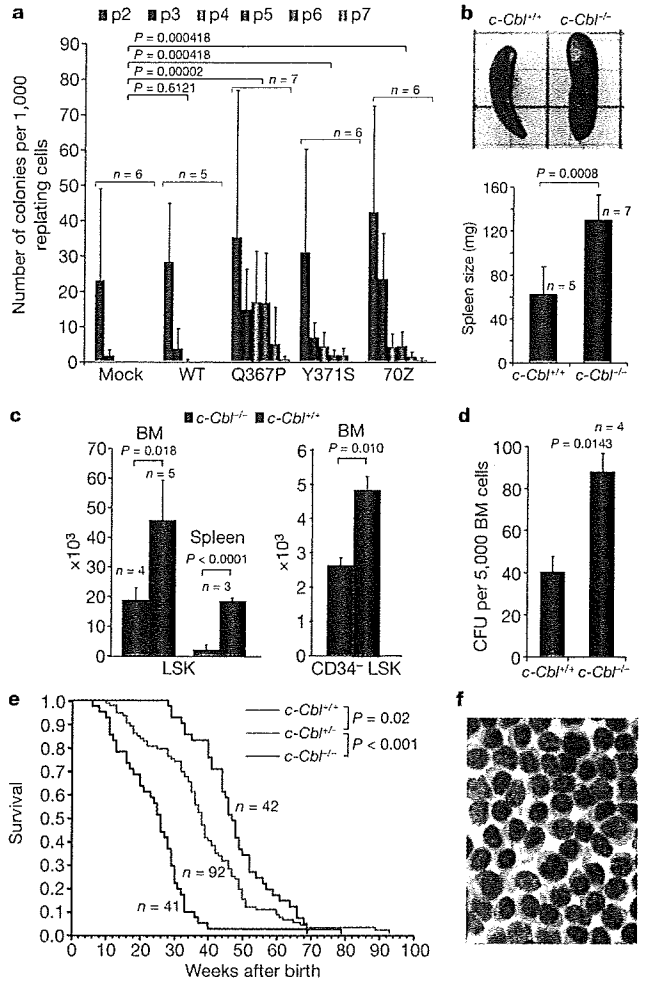

Figure 2 | Tumour-suppressor functions of wild-type C-CBL. **a**, Prolonged replating capacity of LSK cells transduced with mutant *C-CBL* (*C-CBL*(Gln367Pro) and *C-CBL*(Tyr371Ser)), compared to mock- or wild-type *C-CBL*-transduced cells. Replating capacity in methylcellulose culture is shown as mean colony number (and s.d.) per 1,000 replating cells at indicated times of replating. p, passage. **b**, Increased spleen mass in *c-Cbl*$^{-/-}$ mice compared to *c-Cbl*$^{+/+}$ mice (mean spleen weight and s.d.). **c**, Mean number of total LSK (left) and CD34-negative LSK (right) cells (plus s.d.) in bone marrow (BM) and/or spleen in *c-Cbl*$^{+/+}$ (blue columns) and *c-Cbl*$^{-/-}$ mice (red columns). Bone marrow cells from bilateral tibias and femurs were counted for each mouse. **d**, Augmented colony-forming potential of bone marrow cells from *c-Cbl*$^{-/-}$ mice (mean colony number and s.d. per 5,000 bone marrow cells). CFU, colony-forming units. **e**, Kaplan–Meier survival curves of *c-Cbl*$^{+/+}$, *c-Cbl*$^{+/-}$ and *c-Cbl*$^{-/-}$ mice carrying a *BCR-ABL* transgene, showing acceleration of blastic crisis in *c-Cbl*$^{+/-}$ and *c-Cbl*$^{-/-}$ mice. **f**, Wright–Giemsa staining of an enlarged lymph node in a *Bcr-Abl*$^{+}$ *c-Cbl*$^{-/-}$ mouse during blastic crisis shows massive infiltrates of immature leukaemic blasts. Original magnification, ×600.

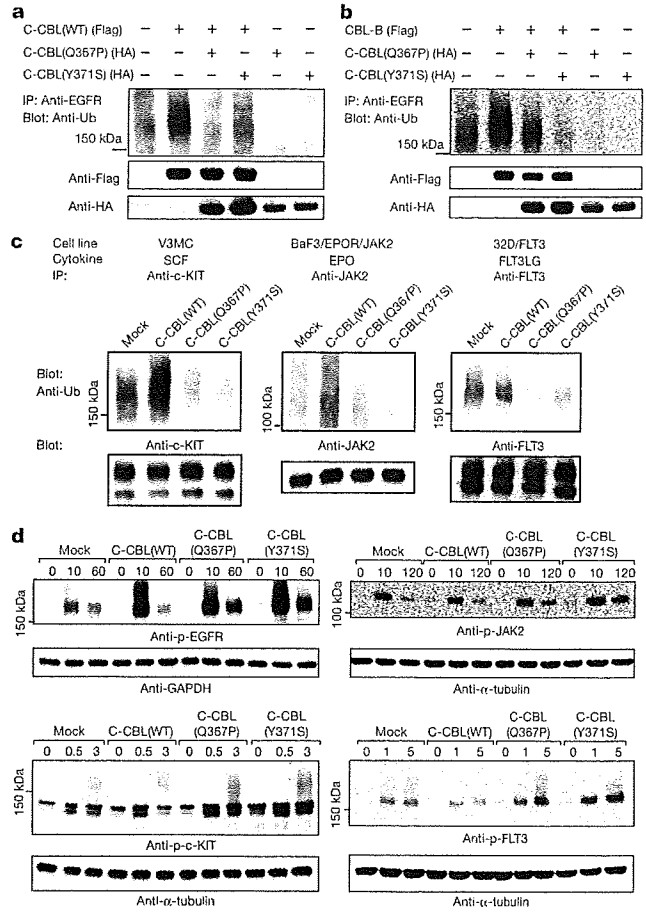

Figure 3 | Inhibitory actions of C-CBL mutants on wild-type C-CBL. **a**, **b**, Flag-tagged wild-type C-CBL (**a**) or CBL-B (**b**) were transfected into NIH3T3 cells stably transduced with human EGFR plus indicated HA-tagged C-CBL mutants. Anti-ubiquitin blots of immunoprecipitated EGFR after EGF stimulation show the inhibitory actions of the C-CBL mutants on ubiquitinating activity of C-CBL (**a**) and CBL-B (**b**). Bottom panels are anti-HA and anti-Flag blots of total cell lysates. **c**, Effects of wild-type and mutant C-CBL on cytokine-induced ubiquitination of c-KIT, JAK2 and FLT3 in haematopoietic cells V3MC, BaF3 co-transduced with human erythropoietin receptor (EPOR) and JAK2 (BaF3/EPOR/JAK2), and FLT3-transduced 32D (32D/FLT3), respectively. Each cell line was further transduced with indicated C-CBL mutants, and ubiquitination of immunoprecipitated kinases was detected by anti-ubiquitin blots at 1 min after stimulation with SCF, EPO and FLT3LG. Anti-kinase blots of the precipitated kinases are shown below each panel. **d**, Kinase phosphorylation was examined at indicated time points (shown in minutes) after ligand stimulation using immunoblot analyses of total cell lysates using antibodies to phosphorylated (p-) EGFR, c-KIT, JAK2 and FLT3 in which anti-α-tubulin or anti-GAPDH blots are provided as a control.

Mouse LSK HSPCs expressed two Cbl family member proteins: wild-type c-Cbl and Cbl-b (Supplementary Fig. 12)[22]. When transduced into NIH3T3 cells stably expressing human epidermal growth factor receptor (EGFR), both Cbl proteins enhanced ubiquitination of EGFR after EGF stimulation, which was suppressed by coexpression of the C-CBL mutants (Fig. 3a, b). In haematopoietic cells, overexpression of wild-type C-CBL enhanced ligand-induced ubiquitination of a variety of tyrosine kinases, including c-KIT, FLT3 and JAK2. In contrast, C-CBL mutants not only showed compromised enzymatic activity, but also inhibited the ubiquitinating activities in these haematopoietic cells (Fig. 3c), leading to prolonged tyrosine kinase activation after ligand stimulation (Fig. 3d).

Because tyrosine kinase signalling is central to cytokine responses in haematopoietic cells and its deregulation is a common feature of myeloproliferative disorders[23], we next examined the effects of *C-CBL* mutations (*C-CBL*(Gln367Pro) and *C-CBL*(Tyr371Ser)) and the loss of wild-type *C-CBL* alleles on the responses of LSK HSPCs to various cytokines. In serum-free conditions, *c-Cbl*$^{-/-}$ LSK cells showed a modestly enhanced proliferative response to a variety of cytokines, including SCF, IL3 and TPO, compared to *c-Cbl*$^{+/+}$ cells (mock columns in Fig. 4a). However, the enhanced response in *c-Cbl*$^{-/-}$ cells was markedly augmented and extended to a broader spectrum of cytokines, including FLT3 ligand by the transduction of *C-CBL* mutants. Of note, the effect of *C-CBL* mutant transduction was not remarkable in *c-Cbl*$^{+/+}$ LSK cells except for the response to SCF, which was clearly enhanced by *C-CBL* mutants

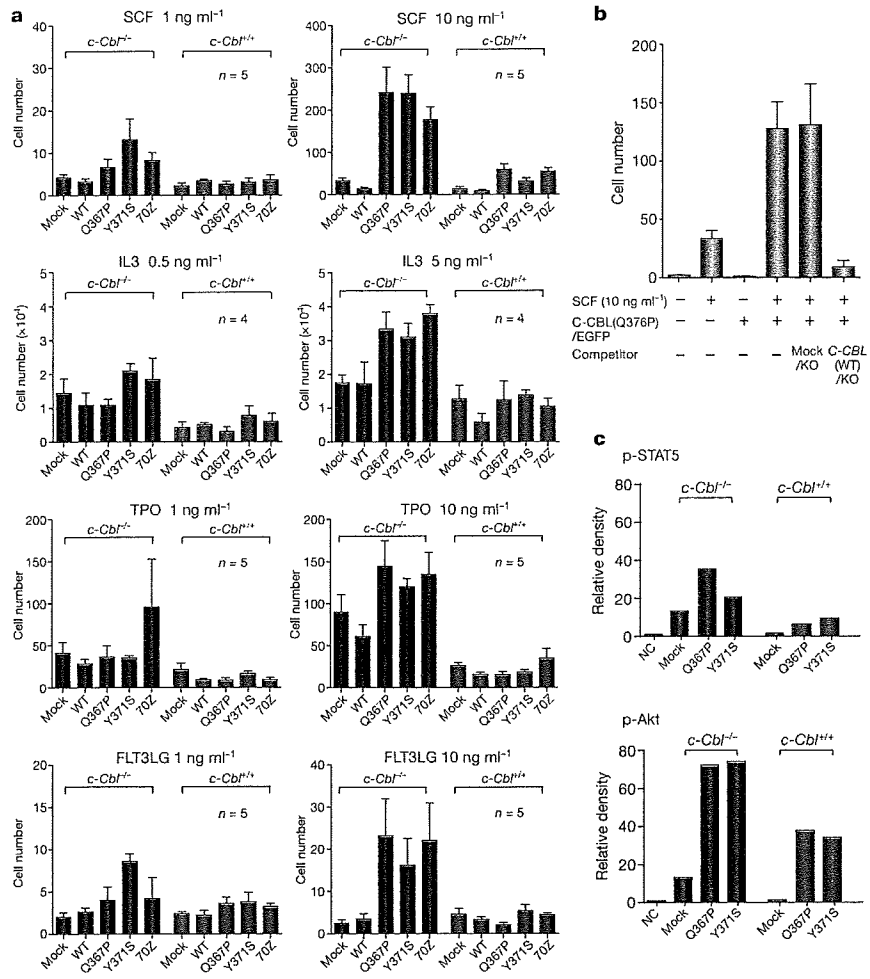

Figure 4 | Gain-of-function of mutant C-CBL augmented by loss of wild-type C-CBL. **a**, *c-Cbl*$^{+/+}$ and *c-Cbl*$^{-/-}$ LSK cells were transfected with various *C-CBL* internal ribosome entry site (IRES)/green fluorescent protein (GFP) constructs, and 50 GFP-positive cells were sorted for serum-free culture containing indicated concentrations of SCF, IL3, TPO and FLT3LG. Mean cell numbers (plus s.e.m.) on day 5 are plotted. **b**, *c-Cbl*$^{-/-}$ LSK cells were co-transduced with C-CBL(Gln367Pro)-IRES-EGFP (C-CBL(Q367P)/EGFP) and mock-IRES-Kusabira-Orange (mock/KO) or wild-type *C-CBL*-IRES-Kusabira-Orange (*C-CBL*(WT)/KO), and 50 GFP/KO double-positive cells were sorted into each well for cell proliferation assays in serum-free culture containing 10 ng ml^{-1} SCF. Mean cell numbers on day 5 (plus s.e.m., $n = 5$) are plotted. **c**, Ten thousand *c-Cbl*$^{+/+}$ and *c-Cbl*$^{-/-}$ LSK cells transduced with various C-CBL constructs were stimulated with 10 ng ml^{-1} SCF and 10 ng ml^{-1} TPO for 15 min. Total cell lysates were analysed by immunoblotting, using antibodies to STAT5, Akt and their phosphorylated forms. The intensities of phosphorylated proteins relative to total STAT5 (top panel) and Akt (bottom panel) are plotted. NC indicates the mean background signal obtained with nonspecific IgG.

even with a *c-Cbl*$^{+/+}$ background (Fig. 4a and Supplementary Fig. 13). To clarify further the effect of wild-type C-CBL on C-CBL mutants, both wild-type C-CBL and C-CBL mutants were co-transduced into *c-Cbl*$^{-/-}$ LSK cells, and their effects on the response to SCF were examined. As shown in Fig. 4b, the hyperproliferative response induced by C-CBL mutants was almost completely abolished by the co-transduction of wild-type C-CBL, suggesting the pathogenic importance of loss of wild-type *C-CBL* alleles found in most *C-CBL*-mutated cases. LSK cells transduced with C-CBL mutants also showed enhanced activation of the STAT5 and Akt pathways on cytokine stimulation (SCF and TPO), which was more pronounced in *c-Cbl*$^{-/-}$ than *c-Cbl*$^{+/+}$ LSK cells (Fig. 4c and Supplementary Fig. 14).

The modest enhancement of sensitivity to cytokines found in *c-Cbl*$^{-/-}$ LSK cells was a consequence of loss of C-CBL functions. In contrast, the hypersensitive response of mutant-transduced *c-Cbl*$^{-/-}$ LSK cells to a broad spectrum of cytokines represents gain-of-function of the mutants that could not be ascribed to a simple loss of C-CBL functions, which was also predicted from the strong association of *C-CBL* mutations with 11q-aUPD by analogy to the gain-of-function *JAK2* mutations associated with 9p-aUPD in polycythemia vera[2]. The gain-of-function of C-CBL mutants became more evident under a *c-Cbl*$^{-/-}$ background. The hypersensitive response to cytokines induced by mutant C-CBL under the *c-Cbl*$^{-/-}$ background was largely offset by the presence of the wild-type *c-Cbl* allele or by the transduction of the wild-type C-CBL gene, suggesting that the gain-of-function could be closely related to loss of C-CBL-like functions, probably by inhibition of Cbl-b. Supporting this view is a previous report that *c-Cbl/Cbl-b* double knockout T cells showed more profound impairments in the downregulation of the T-cell receptor (TCR), more sustained TCR signalling, and more vigorous proliferation, than *c-Cbl* or *Cbl-b* single knockout T cells after anti-CD3 (also known as CD3e) stimulation[24]. This is analogous to the gain-of-function found in some TP53 mutants, which has been explained by functional inhibition of two TP53 homologues, TP73 and TP63 (refs 25, 26). Of note, TP53 was also originally isolated as an oncogene through its mutated forms[27]. The Cbl-b inhibition-based gain-of-function model could be tested directly by comparing the behaviour of *c-Cbl/Cbl-b* double knockout LSK cells with that of LSK cells carrying homozygously knocked-in mutant *C-CBL* alleles. On the other hand, there remains a possibility that the gain-of-function could be mediated by a mechanism other than the simple inhibition of the homologue, because C-CBL mutants retained several motifs

that interacted with numerous signal-transducing molecules. Furthermore, considering the ubiquitous expression of CBL proteins, it would be of interest to explore the possible involvement of mutations in all *CBL* family members in other human cancers.

METHODS SUMMARY

Genomic DNA from 222 bone marrow samples with myeloid neoplasms were analysed using GeneChip SNP-genotyping microarrays (Affymetrix GeneChip) as described[28]. Allelic imbalances were detected from the allele-specific copy numbers calculated using CNAG/AsCNAR software (http://www.genome.umin.jp)[9,10]. *C-CBL* mutations were examined by sequencing PCR-amplified genomic DNA. For functional assays, haemagglutinin (HA)- or Flag-tagged complementary DNAs of wild-type and mutant *C-CBL* were generated by *in vitro* mutagenesis, constructed into a MSCV-based retroviral vector, pGCDNsamIRESGFP or pGCDNsamIRESKO, and used for retrovirus-mediated gene transfer. For the evaluation of oncogenicity of C-CBL mutants, NIH3T3 cells were transfected with various *C-CBL* constructs and used for colony assays in soft agar and tumour formation assays in nude mice. *c-Cbl*-deficient mice were generated using a conventional strategy of gene-targeting and crossed with *BCR-ABL* transgenic mice to evaluate the effect of the *c-Cbl*$^{-}$ allele on the acceleration of blastic crisis. LSK cells sorted from *c-Cbl*$^{+/+}$ and *c-Cbl*$^{-/-}$ mice were transduced with various *C-CBL* constructs. Their responses to cytokines were evaluated by cell proliferation assays, followed by immunoblot analyses of c-KIT, FLT3 and JAK2, as well as their downstream signalling molecules. The effects of C-CBL mutant expression on the ubiquitination of EGFR, c-KIT, FLT3 and JAK2 were examined by transducing C-CBL mutants into relevant cells, followed by anti-ubiquitin blots of the immunoprecipitated kinases after ligand stimulation. Functional competition of C-CBL mutants with wild-type C-CBL was assessed by cell proliferation assays of LSK cells co-transduced with both wild-type and mutant C-CBL genes. This study was approved by the ethics boards of the University of Tokyo, Chang Gung Memorial Hospital and Showa University. Antibodies and primers used in this study are listed in Supplementary Tables 8 and 9.

Full Methods and any associated references are available in the online version of the paper at www.nature.com/nature.

Received 9 October 2008; accepted 30 June 2009.
Published online 20 July 2009.

1. Knudson, A. G. Two genetic hits (more or less) to cancer. *Nature Rev. Cancer* 1, 157–162 (2001).
2. James, C. *et al.* A unique clonal JAK2 mutation leading to constitutive signalling causes polycythaemia vera. *Nature* 434, 1144–1148 (2005).
3. Ryan, P. E. *et al.* Regulating the regulator: negative regulation of Cbl ubiquitin ligases. *Trends Biochem. Sci.* 31, 79–88 (2006).
4. Schmidt, M. H. & Dikic, I. The Cbl interactome and its functions. *Nature Rev. Mol. Cell Biol.* 6, 907–918 (2005).
5. Thien, C. B. & Langdon, W. Y. Cbl: many adaptations to regulate protein tyrosine kinases. *Nature Rev. Mol. Cell Biol.* 2, 294–307 (2001).
6. Thien, C. B. & Langdon, W. Y. c-Cbl and Cbl-b ubiquitin ligases: substrate diversity and the negative regulation of signalling responses. *Biochem. J.* 391, 153–166 (2005).
7. Corey, S. J. *et al.* Myelodysplastic syndromes: the complexity of stem-cell diseases. *Nature Rev. Cancer* 7, 118–129 (2007).
8. Jaffe, E., Harris, N., Stein, H. & Vardiman J. *World Health Organization Classification of Tumours: Pathology and Genetics of Tumours of Haematopoietic and Lymphoid Tissues* 62–73 (IARC Press, 2002).
9. Nannya, Y. *et al.* A robust algorithm for copy number detection using high-density oligonucleotide single nucleotide polymorphism genotyping arrays. *Cancer Res.* 65, 6071–6079 (2005).
10. Yamamoto, G. *et al.* Highly sensitive method for genomewide detection of allelic composition in nonpaired, primary tumor specimens by use of affymetrix single-nucleotide-polymorphism genotyping microarrays. *Am. J. Hum. Genet.* 81, 114–126 (2007).
11. Haase, D. Cytogenetic features in myelodysplastic syndromes. *Ann. Hematol.* 87, 515–526 (2008).
12. Langdon, W. Y. *et al.* v-cbl, an oncogene from a dual-recombinant murine retrovirus that induces early B-lineage lymphomas. *Proc. Natl Acad. Sci. USA* 86, 1168–1172 (1989).
13. Abbas, S. *et al.* Exon 8 splice site mutations in the gene encoding the E3-ligase CBL are associated with core binding factor acute myeloid leukemias. *Haematologica* 93, 1595–1597 (2008).
14. Caligiuri, M. A. *et al.* Novel c-CBL and CBL-b ubiquitin ligase mutations in human acute myeloid leukemia. *Blood* 110, 1022–1024 (2007).
15. Sargin, B. *et al.* Flt3-dependent transformation by inactivating c-Cbl mutations in AML. *Blood* 110, 1004–1012 (2007).
16. Dunbar, A. J. *et al.* 250K single nucleotide polymorphism array karyotyping identifies acquired uniparental disomy and homozygous mutations, including novel missense substitutions of c-Cbl, in myeloid malignancies. *Cancer Res.* 68, 10349–10357 (2008).
17. Zheng, N. *et al.* Structure of a c-Cbl-UbcH7 complex: RING domain function in ubiquitin-protein ligases. *Cell* 102, 533–539 (2000).
18. Murphy, M. A. *et al.* Tissue hyperplasia and enhanced T-cell signalling via ZAP-70 in c-Cbl-deficient mice. *Mol. Cell. Biol.* 18, 4872–4882 (1998).
19. Naramura, M. *et al.* Altered thymic positive selection and intracellular signals in Cbl-deficient mice. *Proc. Natl Acad. Sci. USA* 95, 15547–15552 (1998).
20. Rathinam, C. *et al.* The E3 ubiquitin ligase c-Cbl restricts development and functions of hematopoietic stem cells. *Genes Dev.* 22, 992–997 (2008).
21. Honda, H. *et al.* Acquired loss of p53 induces blastic transformation in p210(bcr/abl)-expressing hematopoietic cells: a transgenic study for blast crisis of human CML. *Blood* 95, 1144–1150 (2000).
22. Zeng, S. *et al.* Regulation of stem cell factor receptor signaling by Cbl family proteins (Cbl-b/c-Cbl). *Blood* 105, 226–232 (2005).
23. Kaushansky, K. Hematopoietic growth factors, signaling and the chronic myeloproliferative disorders. *Cytokine Growth Factor Rev.* 17, 423–430 (2006).
24. Naramura, M. *et al.* c-Cbl and Cbl-b regulate T cell responsiveness by promoting ligand-induced TCR down-modulation. *Nature Immunol.* 3, 1192–1199 (2002).
25. Dittmer, D. *et al.* Gain of function mutations in p53. *Nature Genet.* 4, 42–46 (1993).
26. Lang, G. A. *et al.* Gain of function of a p53 hot spot mutation in a mouse model of Li-Fraumeni syndrome. *Cell* 119, 861–872 (2004).
27. Finlay, C. A., Hinds, P. W. & Levine, A. J. The p53 proto-oncogene can act as a suppressor of transformation. *Cell* 57, 1083–1093 (1989).
28. Chen, Y. *et al.* Oncogenic mutations of ALK kinase in neuroblastoma. *Nature* 455, 971–974 (2008).

Supplementary Information is linked to the online version of the paper at www.nature.com/nature.

Acknowledgements This work was supported by the Core Research for Evolutional Science and Technology, Japan Science and Technology Agency, a Grant-in-Aid from the Ministry of Health, Labor and Welfare of Japan and from the Ministry of Education, Culture, Sports, Science and Technology, and a grant from National Health Research Institute, Taiwan, NHRI-EX96-9434SI, and NIH-2R01CA026038-30. We thank W. Y. Langdon for providing a human *C-CBL* cDNA. A mast-cell cell line expressing c-KIT V3MC was a gift from M. F. Gurish. We also thank Y. Ogino and K. Fujita for their technical assistance.

Author Contributions M.S. and M.Kato performed microarray experiments and subsequent data analyses. T.S., T.Y., H.Honda and H.Hirai generated and analysed *c-Cbl*-null mice. M.S., M.Otsu, S.Y., M.N., K.K., N.G., M.Onodera, M.S.-Y. and H.N. conducted functional assays of C-CBL mutants. L.-Y.S., M.S., M.Kato, K.N., J.T. and A.T. performed mutation analysis. H.O. performed pathological analysis of *c-Cbl*-null mice. L.-Y.S., N.K., H.Harada, M.Kurokawa, S.C., H.M., H.P.K. and M.Omine prepared MDS specimens. M.S., M.Otsu, Y.H., K.O., H.M., H.N., L.-Y.S., H.P.K. and S.O. designed the overall study, and S.O. wrote the manuscript. All authors discussed the results and commented on the manuscript.

Author Information Full copy number data for the 222 samples are accessible from the Gene Expression Omnibus public database (http://ncbi.nlm.nih.gov/geo/) with the accession number GSE15187. Reprints and permissions information is available at www.nature.com/reprints. Correspondence and requests for materials should be addressed to S.O. (sogawa-tky@umin.ac.jp) or L.-Y.S. (sly7012@adm.cgmh.org.tw).

METHODS

Genome-wide analysis of allelic imbalances in primary myeloid neoplasms. Bone marrow specimens were obtained from 222 patients diagnosed with myeloid neoplasms according to the WHO classification (Supplementary Tables 1 and 2). High molecular weight genomic DNA was extracted and used for microarray analysis using Affymetrix GeneChip 50K XbaI, HindIII or 250K NspI, according to the manufacturer's instructions. Genome-wide detection of allelic imbalances was performed using CNAG/AsCNAR software (http://www.genome.umin.jp)[9,10].

Mutation analysis. Mutation analysis was performed by direct sequencing of PCR-amplified coding exons of the relevant genes, using an ABI PRISM 3100 genetic analyser (Applied Biosystems). The target genes, exons and PCR primers are listed in Supplementary Table 8. Tandem duplication of the *FLT3* gene was examined by genomic PCR and sequencing.

Preparation of high-titre vesicular stomatitis virus glycoprotein (VSV-G)-pseudotyped retroviral particles. HA-tagged human *C-CBL* cDNA was a gift from W. Y. Langdon. Nine mutant cDNAs of *C-CBL*, including eight from patients' specimens and a 70Z mutant corresponding to a mutant isolated from mouse lymphoma[29], were generated on the basis of this construct, using a QuickChange site-directed mutagenesis kit (Stratagene). These were then constructed into the retrovirus vectors pGCDNsamIRESGFP and pGCDNsamIRESKO[30–32]. Vector plasmids were co-transfected with a VSV-G cDNA into 293GP cells (provided by R. C. Mulligan) to obtain retrovirus-containing supernatant, which was then transduced into 293GPG cells to establish stable cell lines capable of producing VSV-G-pseudotyped retroviral particles on induction[33,34]. The average titre of retrovirus stocks prepared from these cell lines routinely exceeded approximately $1–10 \times 10^7$ inclusion-forming units per ml, as estimated using Jurkat cells.

Assays for anchorage-independent growth and tumorigenicity in nude mice. NIH3T3 cells (the Japan Cell Resource Bank) were stably transduced with wild-type and mutant *C-CBL* by retrovirus-mediated gene transfer. For colony formation assays, 1.0×10^3 stable cells for each construct were inoculated in 0.33% top agar, and the numbers of colonies >1 mm in diameter were counted 3 weeks after inoculation ($n = 8$). Experiments were repeated four times. For tumour formation in nude mice, 1.0×10^7 stable cells were inoculated subcutaneously at two sites per mouse. Cells were inoculated at six sites in three mice for each construct.

Purification of LSK HSPCs. LSK HSPCs were purified from bone marrow and spleen as described[35,36]. Multicolour flow cytometry analysis and cell sorting were performed using a MoFlo cell Sorter (Beckman Coulter). The purity of sorted cell fractions consistently exceeded 98%.

Replating assays of bone marrow progenitor cells. Bone marrow LSK cells were infected with IRES/GFP-containing retrovirus carrying mock, wild-type C-CBL and three C-CBL mutants (C-CBL(Gln367Pro), C-CBL(Tyr371Ser) and C-CBL(Cys384Gly)) as well as C-CBL(70Z) on RetroNectin-coated dishes. After 48 h infection in culture in StemSpan supplemented with SCF (50 ng ml^{-1}; Peprotech), TPO (20 ng ml^{-1}) and FLT3LG (20 ng ml^{-1}), 1.0×10^2 GFP-positive cells were inoculated in MethoCult M3231 supplemented with TPO (20 ng ml^{-1}), IL3 (10 ng ml^{-1}), IL6 (10 ng ml^{-1}), FLT3LG (10 ng ml^{-1}) and SCF (50 ng ml^{-1}) for colony formation. Colony-forming cells were collected 7 days after each inoculation, from which 1.0×10^3 cells were repeatedly subjected to replating until no colonies were produced. Experiments were repeated at the indicated times for each C-CBL construct.

Generation of *c-Cbl*$^{-/-}$ mice and evaluation of their tumour-prone phenotype. *c-Cbl*$^{-/-}$ mice were generated using a conventional method of gene targeting (Supplementary Fig. 10). *c-Cbl*$^{+/+}$, *c-Cbl*$^{+/-}$ and *c-Cbl*$^{-/-}$ mice were crossed with *BCR-ABL* transgenic mice, and their survival and the development of blastic crises were monitored.

Evaluation of haematopoietic pool size in *c-Cbl*$^{-/-}$ mice. LSK and CD34$^-$ LSK cells were sorted from bone marrow cells or spleens of *c-Cbl*$^{-/-}$ mice, and their numbers were compared to those in *c-Cbl*$^{+/+}$ littermates (8 week old). Approximately 5×10^3 bone marrow cells collected from *c-Cbl*$^{+/+}$ and *c-Cbl*$^{-/-}$ mice were inoculated into MethoCult M3231 culture supplemented with TPO (20 ng ml^{-1}), IL3 (10 ng ml^{-1}), IL6 (10 ng ml^{-1}), EPO (3 U ml^{-1}) and SCF (50 ng ml^{-1}). The number of colonies was counted 7 days after culturing.

***In vitro* cell proliferation assays.** Approximately 6×10^3 LSK cells from *c-Cbl*$^{-/-}$ mice and their *c-Cbl*$^{+/+}$ littermates (8 week old) were sorted into RetroNectin-coated 96-well U-bottom plates containing α-minimum essential medium supplemented with 1% fetal bovine serum (FBS), mouse SCF (50 ng ml^{-1}), and human TPO (100 ng ml^{-1}). After 24 h pre-incubation, retrovirus supernatant was added to each well at a multiplicity of infection of about 10. The plates were incubated for another 24 h in the presence of protamine sulphate (10 μg ml^{-1}), followed by repeated infection and extended culture for 2 days in S-Clone SF-O3 medium (Sanko Junyaku) supplemented with 1% BSA, 50 ng ml^{-1} SCF and 50 ng ml^{-1} TPO. On day 4, fluorescent-marker-positive cells were sorted for subsequent analyses. Cell survival and proliferation of LSK cells transduced with different *C-CBL* constructs were assessed in serum-free liquid culture in 96-well U-bottom plates in the presence of various cytokines. Each well received 50 fluorescent-marker-positive LSK cells, and the cells were cultured in S-Clone supplemented with 1% BSA plus SCF, TPO, IL3 or FLT3LG at the indicated concentrations. Cell numbers were counted either by analysing well images or by flow cytometry using FlowCount beads (Beckman Coulter). After 6 h serum starvation, 1×10^4 LSK cells transduced with various *C-CBL* constructs were stimulated with SCF (10 ng ml^{-1}) and TPO (10 ng ml^{-1}) for 15 min. Whole-cell lysates were examined for activation of STAT5 and Akt by immunoblots using the respective antibodies.

Immunoblot analysis of physical interactions between mutant C-CBL and CBL-B. Flag-tagged CBL-B or C-CBL was co-transfected into NIH3T3 cells with each of three HA-tagged C-CBL mutants (C-CBL(Gln367Pro), C-CBL(Tyr371Ser) and C-CBL(70Z)). Total cell lysates of these NIH3T3 cells were immunoprecipitated with anti-Flag antibody, followed by immunoblot analysis with anti-HA antibody.

Detection of ubiquitination and phosphorylation of kinases. After overnight serum starvation, NIH3T3 cells stably transduced with human EGFR, and indicated HA-tagged C-CBL mutants and Flag-tagged wild-type C-CBL were stimulated with human EGF (10 ng ml^{-1}) for 2 min. Cell lysates were immunoprecipitated with anti-EGF antibody, followed by immunoblotting using anti-ubiquitin antibody. Constructs for wild-type C-CBL and mutant C-CBL were stably transduced into a mast cell line, V3MC, FLT3-transduced 32D cells (32D/FLT3) and BaF3 cells transduced with human EPOR and JAK2 (BaF3/EPOR/JAK2) using retrovirus-mediated gene transfer. After overnight serum starvation, the transduced cells were stimulated with 10 ng ml^{-1} SCF (V3MC), 10 U ml^{-1} EPO (BaF3/EPOR/JAK2) or 10 ng ml^{-1} FLT3LG (32D/FLT3) for 1 min. The specific kinases were immunoprecipitated with relevant antibodies, and their ubiquitination was detected by immunoblotting with anti-ubiquitin antibody. Tyrosine phosphorylation of EGFR, c-KIT, JAK2 and FLT3 was examined by immunoblot analyses of total cell lysates after cytokine stimulation at indicated time points, using antibodies specifically recognizing phosphorylated kinases, anti-p-EGFR, anti-p-c-KIT, anti-p-JAK2 and anti-p-FLT3, respectively. Anti-GAPDH or anti-α-tubulin immunoblot was performed as a control. Antibodies used in this study are listed in Supplementary Table 9.

Statistical analysis. Statistical significance of prolonged replating capacity of mutant *C-CBL*-transduced LSK cells was tested by counting the total number of dishes that produced colonies, followed by Fisher's exact test. Survival curves of *c-Cbl*$^{+/+}$, *c-Cbl*$^{+/-}$ and *c-Cbl*$^{-/-}$ mice containing the *BCR-ABL* transgene were generated using the Kaplan–Meier method. Overall survivals of *C-CBL*-mutated and non-mutated CMML cases were analysed according to the proportional hazard model, using STATA software. Statistical differences in survival were evaluated using the log-rank test, and statistical differences in 2×2 contingency tables were tested according to Fisher's exact method. Student's *t*-tests were used to evaluate the significance of difference in spleen mass, number of haematopoietic progenitors and colony-forming cells between *c-Cbl*$^{+/+}$ and *c-Cbl*$^{-/-}$.

29. Blake, T. J. *et al.* The sequences of the human and mouse c-cbl proto-oncogenes show v-cbl was generated by a large truncation encompassing a proline-rich domain and a leucine zipper-like motif. *Oncogene* 6, 653–657 (1991).
30. Hamanaka, S. *et al.* Stable transgene expression in mice generated from retrovirally transduced embryonic stem cells. *Mol. Ther.* 15, 560–565 (2007).
31. Nabekura, T. *et al.* Potent vaccine therapy with dendritic cells genetically modified by the gene-silencing-resistant retroviral vector GCDNsap. *Mol. Ther.* 13, 301–309 (2006).
32. Sanuki, S. *et al.* A new red fluorescent protein that allows efficient marking of murine hematopoietic stem cells. *J. Gene Med.* 10, 965–971 (2008).
33. Ory, D. S., Neugeboren, B. A. & Mulligan, R. C. A stable human-derived packaging cell line for production of high titer retrovirus/vesicular stomatitis virus G pseudotypes. *Proc. Natl Acad. Sci. USA* 93, 11400–11406 (1996).
34. Suzuki, A. *et al.* Feasibility of *ex vivo* gene therapy for neurological disorders using the new retroviral vector GCDNsap packaged in the vesicular stomatitis virus G protein. *J. Neurochem.* 82, 953–960 (2002).
35. Ema, H. *et al.* Adult mouse hematopoietic stem cells: purification and single-cell assays *Nature Protoc.* 1, 2979–2987 (2006).
36. Osawa, M. *et al.* Long-term lymphohematopoietic reconstitution by a single CD34-low/negative hematopoietic stem cell. *Science* 273, 242–245 (1996).

Cancer Science
The official journal of the Japanese Cancer Association

Dual antitumor mechanisms of Notch signaling inhibitor in a T-cell acute lymphoblastic leukemia xenograft model

Shigeo Masuda,[1,2,3] Keiki Kumano,[1,2] Takahiro Suzuki,[1,2] Taisuke Tomita,[4] Takeshi Iwatsubo,[4,5] Hideaki Natsugari,[6] Arinobu Tojo,[7] Makoto Shibutani,[8] Kunitoshi Mitsumori,[8] Yutaka Hanazono,[3] Seishi Ogawa,[1,9] Mineo Kurokawa[2] and Shigeru Chiba[1,10,11]

[1]Department of Cell Therapy and Transplantation Medicine, University of Tokyo Hospital, Tokyo; [2]Department of Hematology and Oncology, Graduate School of Medicine, University of Tokyo, Tokyo; [3]Division of Regenerative Medicine, Center for Molecular Medicine, Jichi Medical University, Tochigi; [4]Department of Neuropathology and Neuroscience, Graduate School of Pharmaceutical Sciences, University of Tokyo, Tokyo; [5]Department of Neuropathology, Graduate School of Medicine, University of Tokyo, Tokyo; [6]Department of Rational Medicinal Science, Graduate School of Pharmaceutical Sciences, University of Tokyo, Tokyo; [7]Department of Hematology and Oncology, Institute of Medical Sciences, University of Tokyo, Tokyo; [8]Laboratory of Veterinary Pathology, Tokyo University of Agriculture and Technology, Tokyo; [9]21th Century COE Program, Graduate School of Medicine, University of Tokyo, Tokyo; [10]Department of Clinical and Experimental Hematology, Graduate School of Comprehensive Human Sciences, University of Tsukuba, Tsukuba, Japan

(Received May 04, 2009/Revised August 19, 2009/Accepted August 21, 2009/Online publication September 23, 2009)

Constitutive activation of Notch signaling is required for the proliferation of a subgroup of human T-cell acute lymphoblastic leukemias (T-ALL). Previous *in vitro* studies have demonstrated the therapeutic potential of Notch signaling inhibitors for treating T-ALL. To further examine this possibility, we applied a γ-secretase inhibitor (GSI) to T-ALL xenograft models. Treatment of established subcutaneous tumors with GSI resulted in partial or complete regression of tumors arising from four T-ALL cell lines that were also sensitive to GSI *in vitro*. To elucidate the mechanism of action, we transduced DND-41 cells with the active form of Notch1 (aN1), which conferred resistance to *in vitro* GSI treatment. Nevertheless, *in vivo* treatment with GSI induced a partial but significant regression of subcutaneous tumors that developed from aN1-transduced DND-41 cells, whereas it induced complete regression of tumors that developed from mock-transduced DND-41 cells. These findings indicate that the remarkable efficacy of GSI might be attributable to dual mechanisms, directly via apoptosis of DND-41 cells through the inhibition of cell-autonomous Notch signaling, and indirectly via disturbance of tumor angiogenesis through the inhibition of non-cell-autonomous Notch signaling. (*Cancer Sci* 2009; 100: 2444–2450)

The Notch signaling pathway has a crucial role in a variety of cellular functions, including cell proliferation, differentiation, and apoptosis.[1,2] Notch proteins are heterodimeric transmembrane receptors composed of an extracellular subunit and a transmembrane subunit, and associate with each other via heterodimerization (HD) domains in the extracellular regions. Notch signaling, initiated by receptor-ligand interactions, requires subsequent proteolytic cleavage of the receptor by several proteases, resulting in liberation of the cleaved form of Notch1 that is functionally active (hereafter referred to as aN1) as it translocates into the nucleus and up-regulates the transcription of Notch-RBP-Jκ-regulated genes.[3]

Recent studies in tumorigenesis of hematologic malignancies and solid tumors have revealed several examples of aberrant Notch signaling.[2,4,5] Forced expression of aN1 in mouse bone marrow results in the development of T-cell leukemia,[6] and more importantly, amplified Notch signaling contributes to approximately 50% of human T-cell acute lymphoblastic leukemia (T-ALL).[7,8] The Notch signal amplification in T-ALL is due to gain-of-function mutations in the *NOTCH1* gene, which have also been detected in many different murine T-ALL models.[9–12] *NOTCH1* activating mutations cluster at the HD and intracellular domains, leading to ligand-independent cleavage and activation of Notch1, and increased stability of aN1, respectively. Notch1 signaling, whether initiated by receptor–ligand interactions or triggered by *NOTCH1*-activating mutations in the HD domains, eventually depends on the proteolytic activity of γ-secretase. γ-Secretase inhibitors (GSIs), available as small molecular compounds, suppress Notch signaling by blocking the activity of the γ-secretase complex.[13] Previous studies have demonstrated that blockade of Notch signaling with GSI induces cell cycle arrest and apoptosis in a subset of human T-ALL cell lines,[7,14,15] and an early phase clinical trial has already been conducted.[16] Despite that, precise mechanisms of action of GSI on T-ALL *in vivo* are yet to be elucidated.

Here, to examine the potential clinical applications for GSIs in T-ALL patients, and to evaluate the mechanisms of GSI action, we investigated the effects of the GSI compound YO01027[17] (referred to hereafter as YO) on human T-ALL growth in murine xenograft models, because YO administration to mice induced defective melanocyte stem cell maintenance but kept the mice otherwise healthy as shown in our previous paper.[18] The results here indicated that YO is highly effective against T-ALL growth *in vivo* and demonstrated that the efficacy of GSI might be due to the inhibition of Notch signaling via two mechanisms.

Materials and Methods

Cell cultures and reagents. Human T-ALL cell lines (ALL-SIL, DND-41, HPB-ALL, KOPT-K1, TALL-1, MOLT-4, PF-382, and CEM) were obtained from the Fujisaki Cell Center, Hayashibara Biochemical Laboratories (Okayama, Japan), maintained in RPMI supplemented with 10% fetal bovine serum and penicillin/streptomycin, and incubated at 37°C with 5% CO_2. Human umbilical vein endothelial cells (HUVEC; Lonza Walkersville, Walkersville, MD, USA) were cultured in Endothelial Basal Medium-2 (Lonza Walkersville) and SingleQuots (Lonza Walkersville). The YO, which is an LY-411,575 analogue, was synthesized as described previously.[17] YO was dissolved in dimethyl sulfoxide (DMSO) to create 10 mM or 50 mM stock solutions.

Animals. SCID mice (C.B-17/Icr-*scid*/*scid*Jcl; 6 weeks old, female) were purchased from CLEA Japan (Tokyo, Japan) and

[11]To whom correspondence should be addressed. E-mail: schiba-tky@umin.net

doi: 10.1111/j.1349-7006.2009.01328.x

maintained under specific pathogen-free conditions. All experimental procedures were performed in accordance with the guidelines for animal experiments of the University of Tokyo and Jichi Medical University.

Xenograft mouse model. SCID mice at 6–8 weeks of age were inoculated subcutaneously in the right flank with 3×10^7 cells in 300 μL of phosphate buffered saline. In concurrent administration experiments, the mice were assigned to a control group and a YO-treated group the day after tumor inoculation. YO was orally administered daily for at least 30 days at a dose of 0.1 or 1 mg/kg/day. In challenge experiments for established tumors, mice were similarly assigned as described above at approximately 2.5–3 weeks (in HPB-ALL and TALL-1) or 8–12 weeks (in ALL-SIL and DND-41) after tumor cell inoculation, when tumor size had reached a certain volume. YO was orally administered daily at a dose of 0.1, 1, or 10 mg/kg/day. Tumor size was measured at the greatest length and width. The volume was calculated as $1/2 \times$ (tumor length) $\times$ (tumor width)^2.

***In vivo* administration of YO.** *In vivo* administration of YO was performed as described previously.[19] Briefly, 0.1–10 mg/kg of YO or an equal volume of vehicle (DMSO) in 300 μL of 0.5% methylcellulose (Wako, Osaka, Japan) was administered orally to SCID mice using a disposable oral zonde (Fuchigami, Kyoto, Japan) once a day for the indicated periods.

Plasmid construction and retroviral transduction. The cDNA for myc-tagged murine aN1[20] was subcloned into the *Bam*HI restriction site of the retrovirus vector pMYs/internal ribosomal entry site-enhanced green fluorescent protein (IRES-EGFP; pMYs/IG).[21] Retroviral transduction of a human T-ALL cell line, DND-41, was performed using PLAT-F cells as described previously.[21] Following transduction, GFP-positive cells were sorted to 90% purity and used for further analysis. The proteins were detected by Western blotting using an anti-myc antibody (9E10).

Proliferation assay. Cell growth was quantified using a WST-1-based assay (Cell Counting Kit-8; Dojindo Medical Technologies, Kumamoto, Japan), which is a highly sensitive colorimetric assay. Briefly, human T-ALL cell lines (3×10^4 cells/well) or HUVEC (4×10^3 cells/well) were seeded into 96-well plates. Vascular endothelial growth factor (VEGF; 100 ng/mL) was supplemented in the medium for HUVEC. Various concentrations of YO were added, and proliferation was measured in duplicate at 7 days or 11 days using a WST-1-based assay according to the manufacturer's instructions. Proliferation was expressed as a percentage or fold change of vehicle-treated controls. Results are expressed as mean value ± SD.

Detection of apoptosis. Cells were incubated with various concentrations of YO for the indicated periods. Apoptosis was assessed using a fluorescein isothiocyanate-labeled Annexin V staining kit (Immunotech; Beckman-Coulter, Prague, Czech Republic) combined with 7-amino-actinomycin D (7-AAD), according to the manufacturer's instructions, with a FACS Calibur cytometer (BD Biosciences, San Jose, CA, USA).

TUNEL staining. To detect apoptotic cells, ALL-SIL-bearing SCID mice were sacrificed after the treatment with 1 mg/kg YO or vehicle for 5 days. Frozen blocks of tumors were cryosectioned and fixed with 1% paraformaldehyde, followed by analysis for apoptosis using the ApopTag Plus Peroxidase *In Situ* Apoptosis Detection Kit (Millipore, Billerica, MA, USA) according to the manufacturer's instructions.

Western blotting. Western blotting was performed as described previously.[22] The probes used were antibodies against cleaved Notch1 (Val1744; Cell Signaling Technology, Danvers, MA, USA) and GAPDH as a control. The Val1744 antibody was incubated at a dilution of 1:1000 overnight.

Tube formation assay. Upon the BD BioCoat Angiogenesis Plate (96 well), 2×10^4 HUVEC were seeded per well, with or without 100 nM YO. After 18 h, cells were stained with fluores-

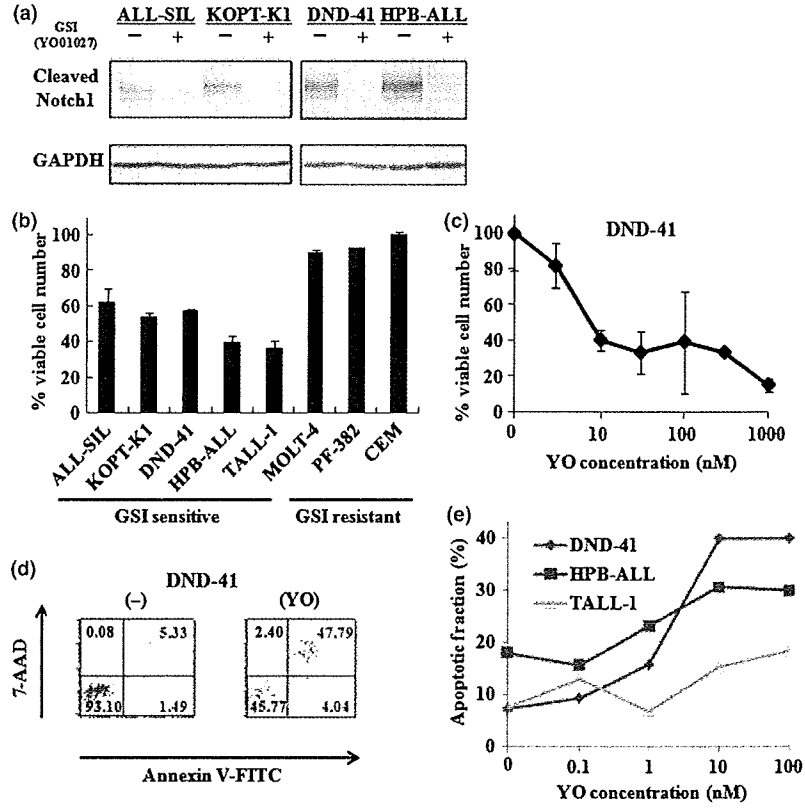

Fig. 1. Inhibition of Notch signaling impairs growth of human T-cell acute lymphoblastic leukemias (T-ALL) cell lines. (a) Western blot analysis for cleaved Notch1 in human T-ALL cell lines treated with 100 nM YO01027 for 48 h. GAPDH is shown as a loading control. (b) Proliferation assay of a panel of human T-ALL cell lines treated for 7 days with 100 nM YO01027 or vehicle control. The percent of viable cell number indicates the proportion of viable cells in the treated populations relative to untreated populations. (c) Dose dependent effects of YO01027 on the proliferation of DND-41 cell line treated for 7 days with 3, 10, 30, 100, 300, 1000 nM YO01027 or vehicle control. The percent of viable cell number indicates the proportion of viable cells in the treated populations relative to untreated populations. (d) Annexin V assay of DND-41 cell line treated for 7 days with 10 nM YO01027 or vehicle control. (e) Dose dependent effects of YO01027 on the apoptosis of human T-ALL cell lines treated for 7 days with 0.1, 1, 10, 100 nM YO01027 or vehicle control. The apoptotic fraction denotes the fraction of Annexin V (+)/7-AAD (+) cells, and the percent of apoptotic fraction indicates the proportion of apoptotic cells among the total cells within each treated well.

cent dye, Calcein AM (BD Biosciences), according to the manufacturer's instructions. Images were captured with the BIOREVO BZ-9000 microscope (Keyence, Osaka, Japan), and the tube length was measured using the BZ-H1C image analysis application (Keyence).

Histological analysis. Frozen blocks were cryosectioned at 5 μm and mounted on slides. Histological sections were air-dried and fixed in acetone for 15 min, followed by immunostaining with a 1:200 dilution of antimouse CD31 antibody (clone; MEC13.3) (BD-Pharmingen, San Diego, CA, USA) overnight at 4°C. Horseradish peroxide with the coloring agent diaminobenzidine was used as the substrate. Sections were then counterstained with hematoxylin. Vessel counting was performed at ×40 magnification in several randomly chosen areas.

Statistics. Statistical analyses were performed using the Student's *t*-test. A *P*-value of <0.05 was considered statistically significant.

Results

Human T-ALL lines are susceptible to Notch inhibition. Some human T-ALL cell lines with *NOTCH1* activating mutations are sensitive to GSI *in vitro*.[7,13–15] We examined the ability of YO, a GSI compound that has not been tested in cell-based experiments, to inhibit Notch signaling. Various human T-ALL cell lines (ALL-SIL, KOPT-K1, DND-41, and HPB-ALL) were treated with YO for 48 h followed by immunoblotting with cleaved Notch1 (Val1744) antibody, which can specifically detect the aN1 proteins. Treatment of these cell lines with 100 nM YO resulted in an almost complete block of Notch1 activity (Fig. 1a).

To investigate the anti-proliferative effect of YO on T-ALL cells, we measured cellular viability using the WST-1-based assay in human T-ALL cell lines after YO treatment. As expected, YO exerted an anti-proliferative effect on some T-ALL cell lines (ALL-SIL, KOPT-K1, HPB-ALL, DND-41, and TALL-1), whereas other cell lines (MOLT-4, PF-382, and CEM) were not sensitive to this compound (Fig. 1b). To examine concentration dependency, DND-41 was treated with various concentrations of YO for 7 days and applied to the WST-1-based assay. A steep concentration dependency was observed between 1 nM and 10 nM. The effect was virtually saturated at >10 nM (Fig. 1c).

Next, we explored whether the decreased proliferation of T-ALL cell lines after treatment with YO was due to the induction of cell cycle arrest and/or apoptosis. We analyzed the cell cycle of the T-ALL cell lines after YO treatment using flow cytometry. As expected from previous reports,[7,13–15] YO induced G0-G1 arrest in all the T-ALL cell lines sensitive to YO (data not shown). Then, we treated five T-ALL cell lines with YO for 7 days followed by Annexin V/7-AAD staining, and found that YO induced significant apoptosis of DND-41 cells (Fig. 1d), as well as the other T-ALL cell lines tested (Fig. 1e). Similar results were observed using a pharmacologically distinct GSI, DAPT, known to block Notch activation (data not shown). Taken together, these results confirmed that some human T-ALL cell lines are susceptible to YO treatment *in vitro*.

Concurrent administration of YO with tumor inoculation results in the inhibition of tumor growth in T-ALL xenograft models. To examine *in vivo* antitumor effects of YO, we used murine xenograft models, in which SCID mice were inoculated subcutaneously with human cell lines. HPB-ALL and TALL-1 cell lines established subcutaneous tumors 2.5–3 weeks after inoculation. The subcutaneous tumors of the YO-treated groups were significantly smaller than those of control groups 2.5–4 weeks after the inoculation and the initiation of concurrent administration of YO or vehicle. Notably, in mice treated with 1 mg/kg of YO, there was no tumor formation observed in

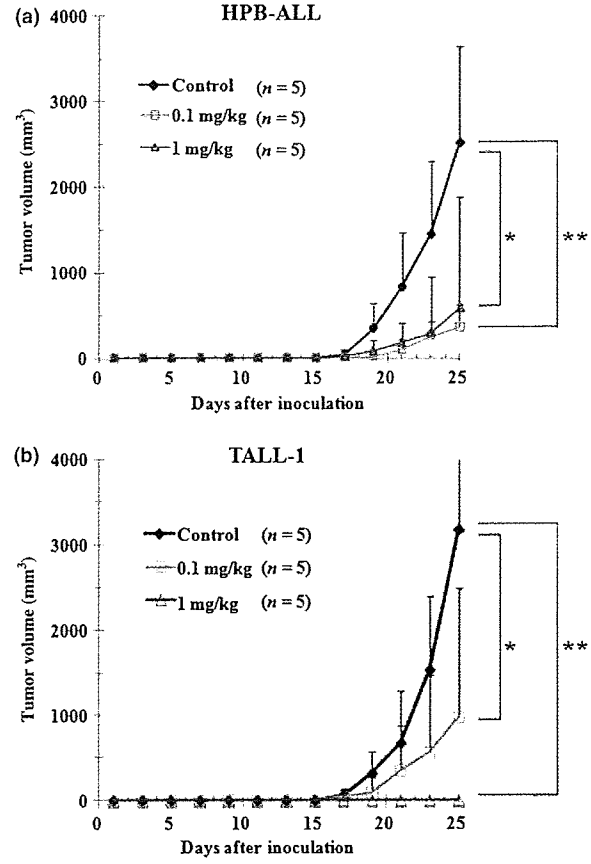

Fig. 2. Antitumor effects of YO01027 (YO) on xenograft models of human T-cell acute lymphoblastic leukemias (T-ALL), with concurrent administration of YO with tumor inoculation. Mice were inoculated subcutaneously with HPB-ALL (a) or TALL-1 cell lines (b). The next day, mice were randomly assigned to receive vehicle alone or varying doses of YO01027 daily, as described in "Materials and Methods". Data represent the mean tumor volume (mm^3) ±SD grown in vehicle-treated mice, YO (0.1 mg/kg)-treated mice, or YO (1 mg/kg)-treated mice. *$P < 0.05$; **$P < 0.01$, statistically significant differences (vehicle *vs* YO).

any of the TALL-1-inoculated mice or in approximately half the HPB-ALL-inoculated mice (Fig. 2a,b). This result indicates that YO exerts *in vivo* antitumor effects on T-ALL, at least during the period of tumor engraftment.

YO treatment against established tumors in T-ALL xenograft models results in partial or complete regression. Next, we evaluated the effects of YO treatment when the tumors grew to visible sizes. In this experimental design, YO treatment resulted in partial (HPB-ALL) or complete (ALL-SIL, DND-41, and TALL-1) regression of the established subcutaneous tumors. When treated with 10 mg/kg/day YO, the growth of tumors derived from HPB-ALL was suppressed to <50% compared with growth without treatment. Tumors derived from ALL-SIL, DND-41, and TALL-1 completely regressed within 2–3 weeks following treatment with YO at 1 mg/kg/day (Fig. 3a).

To confirm the *in vivo* pharmacologic inhibition of Notch signaling by YO, we excised tumors made of ALL-SIL from mice with or without 1 or 10 mg/kg/day YO treatment for 3 days, followed by immunoblotting of the tumor lysates with the Val1744 antibody. The level of cleaved Notch1 was reduced partially or almost completely after 1 or 10 mg/kg/day YO treatment, respectively. Thus, YO administered at both

doi: 10.1111/j.1349-7006.2009.01328.x

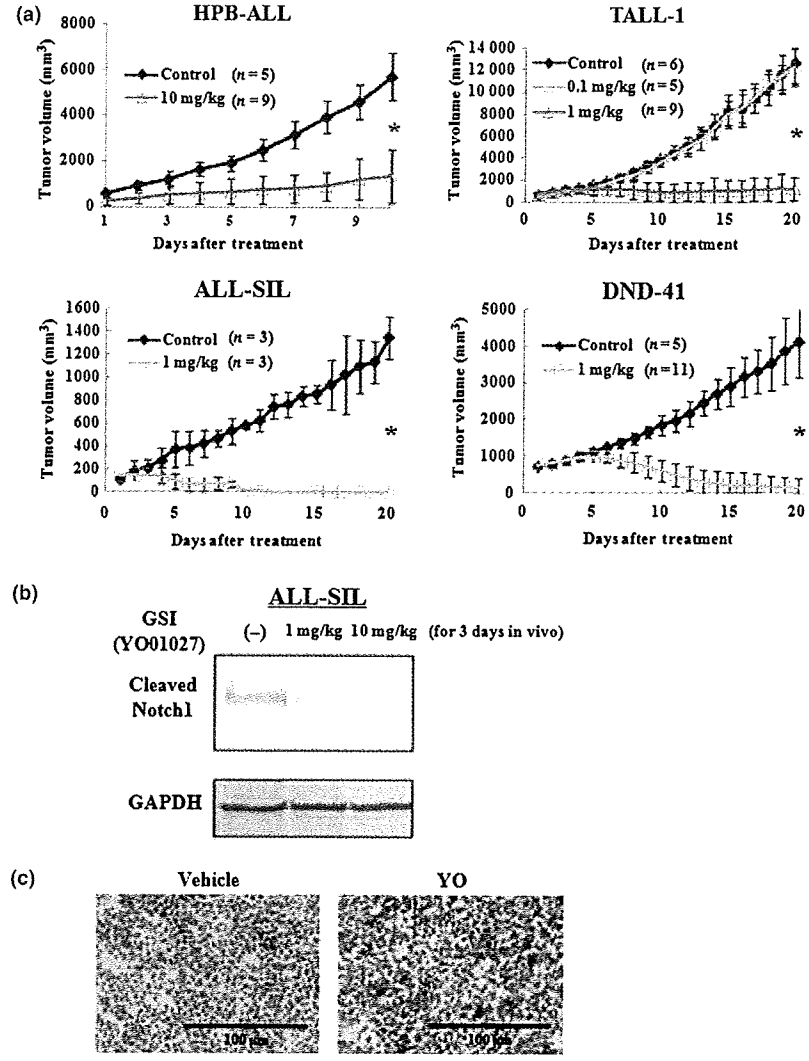

Fig. 3. Antitumor effects of YO01027 (YO) on xenograft models of human T-cell acute lymphoblastic leukemias (T-ALL), with YO treatment after tumor establishment. (a) Mice were inoculated subcutaneously with HPB-ALL, TALL-1, DND-41, or ALL-SIL cell lines. When the diameter of the tumor reached 12–13 mm, mice were randomly assigned to receive vehicle alone or varying doses of YO01027 daily, as described in the "Materials and Methods". Data represent the mean tumor volume (mm^3) ±SD grown in vehicle-treated mice or YO (0.1 or 1 or 10 mg/kg)-treated mice. *$P < 0.001$, statistically significant differences (vehicle *vs* YO). (b) Western blot analysis for cleaved Notch1 in engrafted tumors treated with YO. ALL-SIL-challenged mice were treated daily with vehicle alone or YO, and tumors were harvested 72 h after the initiation of treatment, followed by Western blotting of tumor lysates with cleaved Notch1 (Val1744) antibody. GAPDH is shown as a loading control. (c) YO treatment induces apoptosis of ALL-SIL cells *in vivo*. ALL-SIL-bearing mice were treated daily with vehicle alone or YO01027 at a dose of 1 mg/kg, and tumors were harvested 5 days after the initiation of treatment. Tumor sections were fixed with 1% paraformaldehyde and apoptotic cells were stained using TUNEL assay.

1 mg/kg/day and 10 mg/kg/day to SCID mice was pharmacologically active, and blocked Notch1 signaling partially or almost completely, at least in cells of subcutaneous tumors (Fig. 3b).

To determine whether YO treatment induces apoptosis *in vivo*, we performed TUNEL staining on tumors made of ALL-SIL, which was isolated from vehicle- or YO-treated mice. TUNEL-positive cells were reproducibly increased in number by the YO treatment (Fig. 3c), demonstrating increased apoptosis of T-ALL cells *in vivo*.

Effect of aN1 expression in tumor growth during YO treatment. We next expressed aN1 exogenously in DND-41 cell lines to examine whether aN1 rescues YO-induced cell growth arrest and tumor regression. aN1 represents a protein that is already cleaved, and is thus not a substrate for γ-secretase. Therefore, it was expected that DND-41 cells transduced with aN1 (hereafter referred to as DND-41/aN1) would become resistant to YO treatment.

We established DND-41/aN1 cells by infection of parental DNA-41 cells with aN1-expressing retrovirus, followed by bulk sorting of GFP-positive cells. Expression of aN1 proteins was confirmed by Western blotting with an anti-myc antibody (Fig. 4a). Parental DND-41 and mock-infected DND-41 (DND-41/mock) were sensitive to YO, but, as expected, DND-41/aN1 was substantially resistant to YO *in vitro* when assessed by a cell proliferation assay (Fig. 4b). The continuous presence of 100 nM YO allowed for selection of cells highly resistant to YO (DND-41/aN1/GSI; Fig. 4b). The *in vitro* growth curves of these cells under basal conditions (without YO) were very similar to each other (data not shown).

We implanted parental DND-41, DND-41/mock, DND-41/aN1, and DND-41/aN1/GSI cells subcutaneously into SCID mice. Subcutaneous tumors began to be palpable and the tumor volume reached 700 mm^3 in 8–12 weeks. Treatment with YO at 1 mg/kg/day or control vehicle was then initiated. In vehicle-treated mice, the tumors derived from parental DND-41, DND-41/mock, DND-41/aN1, and DND-41/aN1/GSI cells grew in a similar manner, whereas YO treatment resulted in a substantial regression of the tumors derived from parental DND-41 and DND-41/mock cells (Fig. 4c,d). Interestingly, *in vivo* YO treatment of tumors derived from DND-41/aN1 and DND-41/aN1/GSI cells, which were resistant to YO *in vitro*, induced significantly slower cell growth compared with the vehicle treatment, suggesting that these cells were sensitive to YO to some degree *in vivo* (Fig. 4c,d). In some mice, we observed a stabilization of the tumor volume. Nevertheless, YO treatment was not sufficiently effective on DND-41/aN1 and DND-41/aN1/GSI to regress the tumors to an impalpable level, unlike parental DND-41- and DND-41/mock-derived tumors.

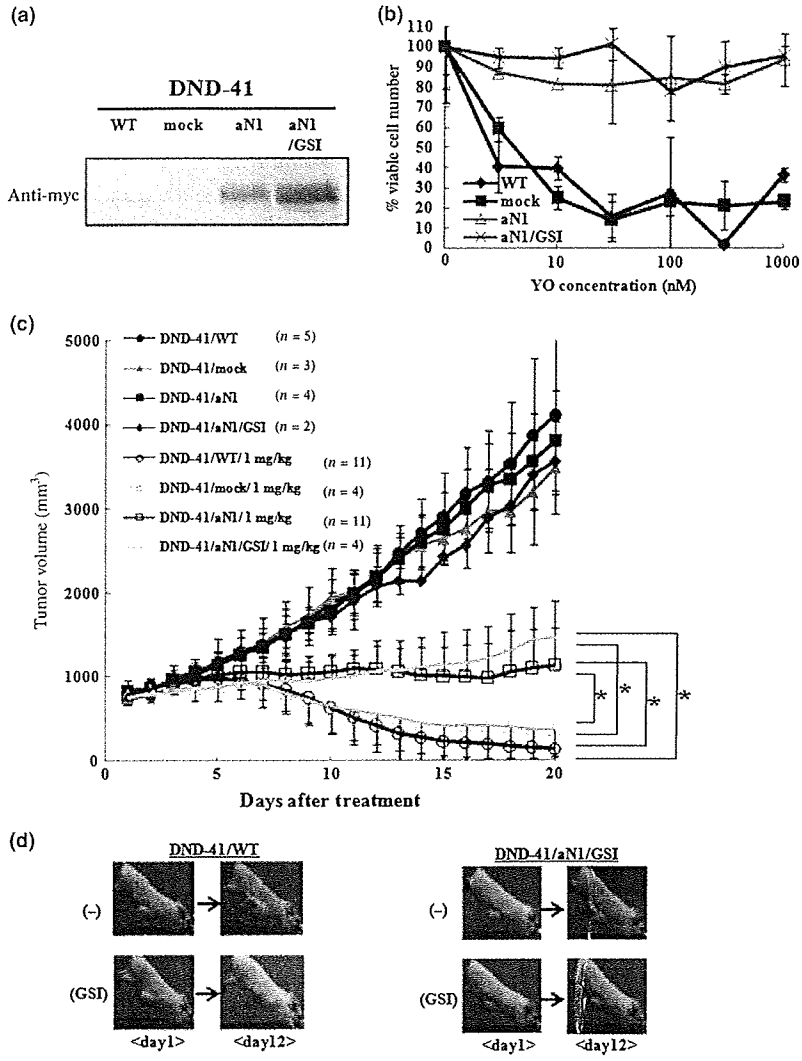

Fig. 4. Establishment of DND-41/aN1 and effects of aN1 rescue on tumor growth during YO01027 (YO) treatment. (a) Expression of aN1 proteins tagged with myc in DND-41/aN1 cells and DND-41/aN1/GSI cells was confirmed by Western blotting analysis. (b) Proliferation assay of established DND-41/aN1 and DND-41/aN1/GSI cell lines, compared with DND-41/WT and DND-41/mock cell lines, after treatment for 11 days with varying doses of YO. The percent of viable cell number indicates the proportion of viable cells in the treated populations relative to untreated populations. (c) Antitumor effects of YO on xenograft models of DND-41/WT, DND-41/mock, DND-41/aN1, and DND-41/aN1/GSI (pre-selected by γ-secretase inhibitor [GSI] *in vitro*). "1 mg/kg/day" denotes the group that received the YO treatment at a dose of 1 mg/kg/day. Data represent the mean tumor volume (mm^3) ±SD of vehicle-treated mice or YO (1 mg/kg)-treated mice. *$P < 0.01$, statistically significant differences. (d) Representative appearance of subcutaneous xenograft models during YO treatment. DND-41 cells stably expressing control vector or aN1 (pre-selected by GSI *in vitro*) were grown as xenografts in SCID mice. Representative mice from each group are shown.

Effect of YO on *in vitro* tube formation and *in vivo* tumor vessels. Recent studies have demonstrated that inhibition of Notch signaling in solid tumors resulted in tumor regression via increased tumor vessels with poor perfusion.[23–26] It has been shown that Notch inhibition leads to promotion of non-functioning angiogenesis.

Tube formation assay was performed to investigate the effect of YO on *in vitro* angiogenesis using HUVEC. We found that YO treatment significantly increased the tube length in the tube formation assay (Fig. 5a,b), suggesting that Notch inhibition promoted proliferation of endothelial cells, which is consistent with previous studies.[24,27] In addition, cell proliferation in the presence of VEGF was measured with WST-1-based assay. YO significantly promoted proliferation of HUVEC (Fig. 5c) as previously reported.[24,27]

To further clarify the mechanism of action with YO treatment, we analyzed the tumor vasculature during YO treatment. We implanted DND-41 cells into SCID mice and started YO or vehicle treatment after the tumor diameter reached approximately 1 cm. We sacrificed mice at treatment day 5, and analyzed tumor sections by immunostaining for anti-CD31, which is able to identify the vessels in tumors. In the average, approximately 30 and >40 vessels per mm^2 were observed in the vehicle-treated and YO-treated mice, respectively (Fig. 5d,e). These results are consistent with the previous reports described above, in which tumor regression would result from increased but poorly functional tumor vessels. Collectively, tumor regression in our models may depend partially on the disrupted tumor vasculature with paradoxically increased tumor vessels presumably through the inhibition of non-cell-autonomous Notch signaling by YO.

Discussion

The findings of the present study confirmed that the YO compound that we synthesized is a GSI that efficiently blocks Notch signaling in T-ALL cell lines carrying activating *NOTCH1* mutations and induces apoptosis of these cell lines *in vitro*. The cell-autonomous effect against Notch signaling described here is postulated to be the mechanism of anti-T-ALL, creating the bases for clinical studies of a GSI targeting T-ALL.

We demonstrated a marked *in vivo* effect of YO in a xenograft model that was more dramatic than we had expected. Although the mechanisms of YO action on T-ALL have been virtually confined to the cell-autonomous Notch signal inhibition, including a recent report describing the combinatorial effect of steroid with GSI,[28] the strong effect of GSI *in vivo* could also be attributed to non-cell-autonomous inhibition of Notch signaling.

Our findings were consistent with the recent reports on the role of Notch signaling in tumor angiogenesis.[23–26] Delta-4, one of the Notch ligands, is expressed on tip cells in the endothe-

doi: 10.1111/j.1349-7006.2009.01328.x

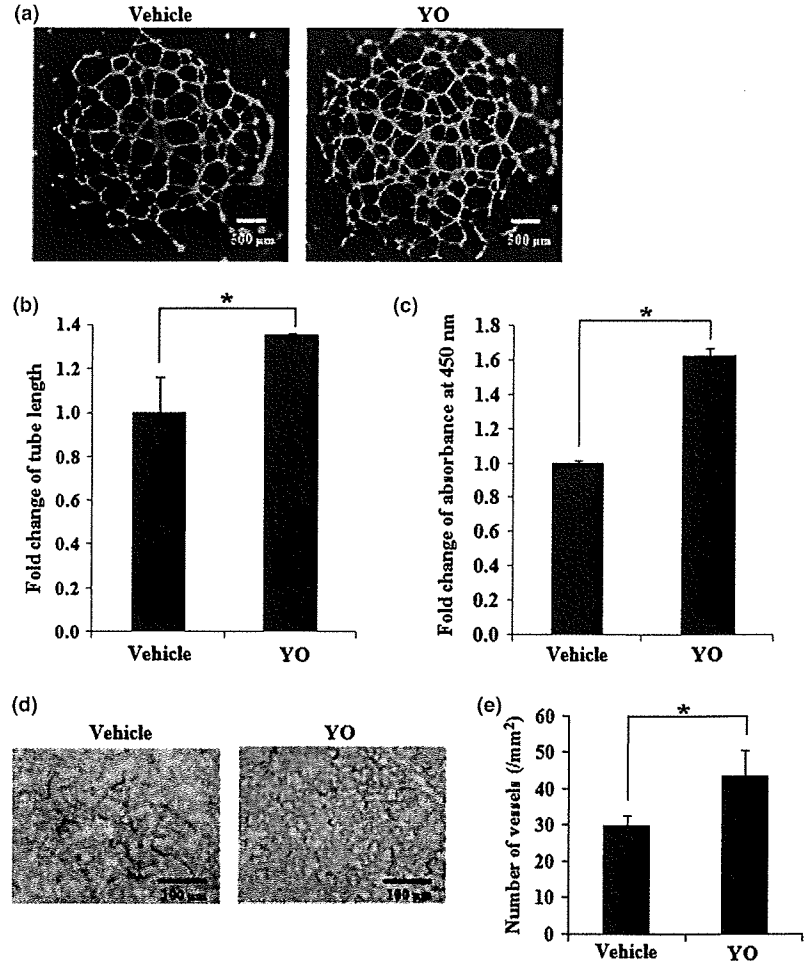

Fig. 5. *In vitro* and *in vivo* analysis of vascular cells after YO01027 (YO) treatment. (a) The *in vitro* tube formation analysis of HUVEC, either with or without 100 nM YO treatment. The cells were stained with fluorescent dye, Calcein AM, and the representative images are shown. Original magnification, ×20. (b) Quantitative analysis of tube length after tube formation of HUVEC with or without 100 nM YO. Fold change of tube length is shown, compared with that of vehicle control. $*P < 0.05$, statistically significant differences. (c) The cell proliferation assay of HUVEC in the presence of vascular endothelial growth factor (VEGF), either with or without 100 nM YO for 7 days. Fold change of absorbance at 450 nm is shown, compared with that of the vehicle control. $*P < 0.05$, statistically significant differences. (d) Anti-CD31 immunostainings of tumor sections in DND-41-bearing SCID mice, either after YO treatment at a dose of 1 mg/kg/day or after vehicle treatment. Original magnification, ×40. (e) Quantitative analysis of vessels in tumors after YO treatment. The cells stained with anti-CD31 were counted, and data represent the mean vessel density (per mm^2) ±SD in tumors derived from DND-41. $*P < 0.05$, statistically significant differences.

lium of newly elongating tumor vessels by stimulation with VEGF. Engagement of Notch1 expressed on the stalk cells in the endothelium by neighboring tip cell-expressing Delta-4 blocks differentiation of the stalk cells into tip cells, which represents the process required for the normally functioning tumor vessel formation. Blockade of this signaling pathway impairs normal tumor angiogenesis and creates hyper-blanched, non-functioning vasculature, which results in regression of the solid tumor. Whereas we used T-ALL cell lines in our experiments, we chose the subcutaneous tumor injection model because it is more convenient for observing and measuring the tumors. In this subcutaneous tumor model, we observed a similar tendency regarding tumor vessel density, from which we could easily speculate that the same mechanism was underlying this phenomenon.

The introduction of the GSI-insensitive cleaved form of Notch1 into DND-41 cells transformed these cells to be completely resistant to YO *in vitro*, exactly as expected, but failed to confer complete resistance to YO in the subcutaneous xenograft model. Whereas the subcutaneous tumors derived from DND-41/aN1 were significantly more resistant to YO than tumors derived from parental DND-41 and DND-41/mock cells, they still significantly responded to YO. These observations fit the idea that the marked *in vivo* antitumor effect of YO against subcutaneous tumors derived from parental DND-41 as well as DND-41/mock cells was mediated through, in addition to the cell-autonomous effect, a blockade of tumor vasculature that supplies blood to the tumor cells in a non-cell-autonomous fashion.

We confirmed that subcutaneous tumors made of a colon cancer cell line, LoVo, which was non-sensitive to YO *in vitro*, were partially regressed by YO at 10 mg/kg/day (data not shown). The effect of YO on the LoVo tumors, however, was not as strong as on tumors made of parental DND-41 and several other T-ALL cell lines, again supporting the idea that the exceptionally strong effect of YO on T-ALL xenografts is due to the inhibiting effect of YO on Notch signaling at two independent targets *in vivo*.

As shown in Figure 3(b), inhibition of Notch1 activation *in vivo* was almost complete with YO at 10 mg/kg but incomplete with YO at 1 mg/kg. On the other hand, the effect of YO *in vitro* was saturated by YO >10 nM, as shown in Figure 1(c). These findings might indicate that >10 nM serum/tissue concentration is achieved with 10 mg/kg and 1–10 nM with 1 mg/kg administration, if both *in vitro* and *in vivo* results are considered together. Whereas administration of YO at 1–3 mg/kg/day for up to 4 weeks did not cause weight loss, diarrhea, or hair coat abnormalities in mice, treatment at 10 mg/kg/day for more than 2 weeks resulted in obvious weight loss, diarrhea, and hair coat roughness. This implies a narrow window of YO for the treatment purpose. Nevertheless, it also indicates that the sensitivity to YO is variable among tissues and cells, and this difference might be important for YO to be considered as a drug. Together with the results described in previous papers,[18,29,30] a subset of T-ALL cells may be the most sensitive among others and possibly similar to melenocyte stem cells and splenic marginal zone B cells. In contrast, thymocyte progenitors and intestinal goblet cells appear to be less sensitive to YO.

Based on the facts that subcutaneous tumors from T-ALL cell lines do not represent common clinical presentations and that

our finding might depend on the experimental model that we chose in this study, the question arises as to how the current findings can be translated to clinical application. The vasculature component might be negligible in the leukemia model, but the effect of the combination of cell-autonomous apoptosis induction in leukemia cells with the inhibition of angiogenesis in leukemic cell-infiltrating bone marrow is not known. The effectiveness of YO in a leukemia model must be examined using the same T-ALL cell lines.

The discovery of *NOTCH1* activating mutations in T-ALL has made the Notch pathway an attractive target for therapy.[31] The results described here indicate the rationale for the use of GSI in the treatment of T-ALL, as well as for solid tumors whose tumor vasculature formation is dependent on Notch signaling.

Nevertheless, resistance of T-ALL against GSI might limit the clinical use of GSI. Recently, mutational loss of the phosphatase and tensin homolog (PTEN) gene, which encodes a key tumor suppressor that inhibits the phosphatidylinositol-3 kinase (PI3K)–Akt signaling pathway, was discovered in T-ALL cells that are resistant to GSI.[32] This could explain the variation of GSI sensitivity among T-ALL cells. Our results with HPB-ALL raise a different issue. This cell line was very sensitive to YO *in vitro*, but subcutaneous tumors derived from HPB-ALL appeared to be less sensitive to YO compared to other cells such as DND-41. This result indicates that YO concentrations sufficient to inhibit Notch1 activation may not be achieved in the subcutaneous tumor made from HPB-ALL. In addition, it is likely that inhibition of tumor vessel formation is less efficient for the reduction of subcutaneous HPB-ALL tumors for some reasons, such that this particular tumor is less dependent on tumor vessels.

Expectations and questions are intermingled with regard to the development of GSI and other Notch signal inhibitors for the treatment of T-ALL as well as other tumors. Nevertheless, various Notch signal inhibitors are being developed aiming at clinical use.

Acknowledgments

We thank Toshio Kitamura (Institute of Medical Science, University of Tokyo) for the pMYs/IRES-EGFP retrovirus vector and Akira Harashima (Hayashibara Biomedical Laboratories) for the T-ALL cell lines (ALL-SIL, DND-41, HPB-ALL, KOPT-K1, TALL-1, MOLT-4, PF-382, and CEM). This work was supported in part by Grants-in-Aid for Scientific Research (KAKENHI nos. 17014023, 18013012, and 19390258) from the Ministry of Education, Culture, Sports, Science and Technology (MEXT) of Japan, and a Research Grant from the Sagawa Foundation of Promotion of Cancer Sciences to S.C.; Grants-in-Aid for Young Scientists (KAKENHI nos. 17790637 and 19790660) from MEXT; research funding for young scientists from the Science and Technology Foundation of Japan; research funding from the Japan Leukemia Research Fund; and research funding from Aichi Cancer Research Foundation to S.M.

References

1 Grabher C, von Boehmer H, Look AT. Notch 1 activation in the molecular pathogenesis of T-cell acute lymphoblastic leukaemia. *Nat Rev Cancer* 2006; **6**: 347–59.
2 Leong KG, Karsan A. Recent insights into the role of Notch signaling in tumorigenesis. *Blood* 2006; **107**: 2223–33.
3 Mumm JS, Kopan R. Notch signaling: from the outside in. *Dev Biol* 2000; **228**: 151–65.
4 Pear WS, Aster JC. T cell acute lymphoblastic leukemia/lymphoma: a human cancer commonly associated with aberrant NOTCH1 signaling. *Curr Opin Hematol* 2004; **11**: 426–33.
5 Lee SY, Kumano K, Nakazaki K *et al.* Gain-of-function mutations and copy number increases of Notch2 in diffuse large B-cell lymphoma. *Cancer Sci* 2009; **100**: 920–6.
6 Pear WS, Aster JC, Scott ML *et al.* Exclusive development of T cell neoplasms in mice transplanted with bone marrow expressing activated Notch alleles. *J Exp Med* 1996; **183**: 2283–91.
7 Weng AP, Ferrando AA, Lee W *et al.* Activating mutations of NOTCH1 in human T cell acute lymphoblastic leukemia. *Science* 2004; **306**: 269–71.
8 Lee SY, Kumano K, Masuda S *et al.* Mutations of the Notch1 gene in T-cell acute lymphoblastic leukemia: analysis in adults and children. *Leukemia* 2005; **19**: 1841–3.
9 Dumortier A, Jeannet R, Kirstetter P *et al.* Notch activation is an early and critical event during T-Cell leukemogenesis in Ikaros-deficient mice. *Mol Cell Biol* 2006; **26**: 209–20.
10 Lin YW, Nichols RA, Letterio JJ, Aplan PD. Notch1 mutations are important for leukemic transformation in murine models of precursor-T leukemia/lymphoma. *Blood* 2006; **107**: 2540–3.
11 O'Neil J, Calvo J, McKenna K *et al.* Activating Notch1 mutations in mouse models of T-ALL. *Blood* 2006; **107**: 781–5.
12 Reschly EJ, Spaulding C, Vilimas T *et al.* Notch1 promotes survival of E2A-deficient T cell lymphomas through pre-T cell receptor-dependent and -independent mechanisms. *Blood* 2006; **107**: 4115–21.
13 Weng AP, Nam Y, Wolfe MS *et al.* Growth suppression of pre-T acute lymphoblastic leukemia cells by inhibition of notch signaling. *Mol Cell Biol* 2003; **23**: 655–64.
14 Lewis HD, Leveridge M, Strack PR *et al.* Apoptosis in T cell acute lymphoblastic leukemia cells after cell cycle arrest induced by pharmacological inhibition of Notch signaling. *Chem Biol* 2007; **14**: 209–19.
15 O'Neil J, Grim J, Strack P *et al.* FBW7 mutations in leukemic cells mediate NOTCH pathway activation and resistance to γ-secretase inhibitors. *J Exp Med* 2007; **204**: 1813–24.
16 Shih IeM, Wang TL. Notch signaling, γ-secretase inhibitors, and cancer therapy. *Cancer Res* 2007; **67**: 1879–82.
17 Fuwa H, Okamura Y, Morohashi Y *et al.* Highly efficient synthesis of medium-sized lactams via intramolecular Staudingeraza-Wittig reaction of w-azido pentafluorophenyl ester: synthesis and biological evaluation of Ly411575 analogues. *Tetrahedron Lett* 2004; **45**: 2323–6.
18 Kumano K, Masuda S, Sata M *et al.* Both Notch1 and Notch2 contribute to the regulation of melanocyte homeostasis. *Pigment Cell Melanoma Res* 2008; **21**: 70–8.
19 Wong GT, Manfra D, Poulet FM *et al.* Chronic treatment with the gamma-secretase inhibitor LY-411,575 inhibits beta-amyloid peptide production and alters lymphopoiesis and intestinal cell differentiation. *J Biol Chem* 2004; **279**: 12876–82.
20 Kumano K, Chiba S, Kunisato A *et al.* Notch1 but not Notch2 is essential for generating hematopoietic stem cells from endothelial cells. *Immunity* 2003; **18**: 699–711.
21 Kitamura T, Koshino Y, Shibata F *et al.* Retrovirus-mediated gene transfer and expression cloning: powerful tools in functional genomics. *Exp Hematol* 2003; **31**: 1007–14.
22 Masuda S, Kumano K, Shimizu K *et al.* Notch1 oncoprotein antagonizes TGF-beta/Smad-mediated cell growth suppression via sequestration of coactivator p300. *Cancer Sci* 2005; **96**: 274–82.
23 Noguera-Troise I, Daly C, Papadopoulos NJ *et al.* Blockade of Dll4 inhibits tumour growth by promoting non-productive angiogenesis. *Nature* 2006; **444**: 1032–7.
24 Ridgway J, Zhang G, Wu Y *et al.* Inhibition of Dll4 signalling inhibits tumour growth by deregulating angiogenesis. *Nature* 2006; **444**: 1083–7.
25 Hellstrom M, Phng LK, Hofmann JJ *et al.* Dll4 signalling through Notch1 regulates formation of tip cells during angiogenesis. *Nature* 2007; **445**: 776–80.
26 Siekmann AF, Lawson ND. Notch signalling limits angiogenic cell behaviour in developing zebrafish arteries. *Nature* 2007; **445**: 781–4.
27 Yamanda S, Ebihara S, Asada M *et al.* Role of ephrinB2 in nonproductive angiogenesis induced by Delta-like 4 blockade. *Blood* 2009; **113**: 3631–9.
28 Real PJ, Tosello V, Palomero T *et al.* Gamma-secretase inhibitors reverse glucocorticoid resistance in T cell acute lymphoblastic leukemia. *Nat Med* 2009; **15**: 50–8.
29 Radtke F, Wilson A, Stark G *et al.* Deficient T cell fate specification in mice with an induced inactivation of Notch1. *Immunity* 1999; **10**: 547–58.
30 Saito T, Chiba S, Ichikawa M *et al.* Notch2 is preferentially expressed in mature B cells and indispensable for marginal zone B lineage development. *Immunity* 2003; **18**: 675–85.
31 Aster JC. Deregulated NOTCH signaling in acute T-cell lymphoblastic leukemia/lymphoma: new insights, questions, and opportunities. *Int J Hematol* 2005; **82**: 295–301.
32 Palomero T, Sulis ML, Cortina M *et al.* Mutational loss of PTEN induces resistance to NOTCH1 inhibition in T-cell leukemia. *Nat Med* 2007; **13**: 1203–10.

doi: 10.1111/j.1349-7006.2009.01328.x

Ann Hematol (2009) 88:811–812
DOI 10.1007/s00277-008-0664-8

LETTER TO THE EDITOR

Hemoperitoneum due to spontaneous rupture of the left gastroepiploic artery in a patient with hemophilia A

Akihide Yoshimi · Tsuyoshi Takahashi · Toru Motokura · Yutaka Yatomi · Shigeru Chiba · Mineo Kurokawa

Received: 21 September 2008 / Accepted: 3 December 2008 / Published online: 18 December 2008

Dear Editor,

We experienced spontaneous rupture of the left gastroepiploic artery (GEA) in a patient with hemophilia A. A 35-year-old male with moderate hemophilia A (factor VIII activity 3%) presented to the emergency room with constant gradually increasing abdominal pain. There was no previous history of trauma. His abdomen was noted to be distended and diffusely tender, without guarding or rebound. His rectal examination was guaiac negative. His initial laboratory evaluation revealed the hemoglobin level of 9.9 g/dl, which had decreased from 14.0 g/dl over the previous 16 days. Roentgenograms of the chest and abdomen were negative. An ultrasound study showed a large pool of peritoneal fluid in the abdomen. Computed tomography (CT) scanning with intravenous contrast revealed pseudovessel and hematoma in greater omentum (Fig. 1a), which showed very active bleeding. CT scanning also showed massive intraperitoneal blood. Intravenous recombinant factor VIII was administered and an angiography was performed immediately. On selective angiography, an extravascular leakage of the contrast medium from a branch of the left GEA was observed (Fig. 1b). A transcatheter arterial embolization (TAE) was performed successfully using micro-coils with gelatin sponge particles. After TAE, the patient was managed with administration of intravenous recombinant factor VIII, leading to an uneventful recovery.

Abdominal apoplexy (AA) is the spontaneous rupture of a visceral artery causing hemoperitoneum. The true incidence of AA is unknown, and the reports on spontaneous GEA rupture are extremely rare. On the other hand, hemorrhage from an artery in a hemophilic patient has rarely been reported and usually secondary to trauma or a medical procedure [1-3]. To the best of our knowledge, AA or rupture of GEA in a hemophilic patient has not yet been reported. Because the incidence of AA or hemophilia is low, it is not clear whether or not hemophilia is a risk factor of AA. There is, at least a possibility that hemophilia aggravated the hemorrhage in the present case. Because AA is a potentially fatal disease even in patients without hematological and/or coagulation abnormalities, it is very important to diagnose and determine the optimal treatment strategy urgently. Physicians should keep in mind that bleeding source can localize in splanchnic arteries and a rupture of these arteries should be included in the differential diagnosis of abdominal pain, especially when a patient has hematological and/or coagulation abnormalities.

Surgical or nonsurgical treatments including ligation, aneurysmectomy, gastrectomy, or embolization are needed for hemorrhage due to a ruptured GEA. TAE has also been reported for visceral artery bleeding. This is a safe and less invasive procedure than surgery, although recanalization or rerupture have been reported to occur in a few patients, necessitating reembolization [4]. The diagnosis in our patients could be confirmed by angiography immediately, and TAE was performed successfully. Therefore, angiography and TAE were very effective in the present case.

A. Yoshimi · T. Takahashi · T. Motokura · S. Chiba · M. Kurokawa (✉)
Department of Hematology and Oncology,
Graduate School of Medicine, University of Tokyo,
7-3-1 Hongo, Bunkyo-ku,
Tokyo 113-8655, Japan
e-mail: kurokawa-tky@umin.ac.jp

Y. Yatomi
Department of Clinical Laboratory,
University of Tokyo Hospital,
Tokyo, Japan